SPACECRAFT MAGNETIC CLEANLINESS ANALYSIS SOFTWARE
GAMAG

K. Mehlem, PhD, Msc
Astos Solution GmbH
Stuttgart, Germany
www.astos.de

List of content

1. Basic Tasks of the GAMAG Software

Spacecraft have in general many magnetic parts like thrusters, TWT's, motors, current loops etc. For spacecraft that carry magnetometer experiments, like Giotto, Ulysses, Cluster, Cassini etc. a stringent Magnetic Cleanliness Specification has to be met, for instance 0.1 nT at the boom tip.

For all other spacecraft which have some pointing accuracy specifications and which are flying in strong magnetic environments like around the Earth, Jupiter, Saturn etc., the Attitude Control System (ACS) has to be dimensioned according to the Global Dipole Moment of the spacecraft.

The main tasks of the **GAMAG** software are basically two-fold:

➢ Verify the Magnetic Field Cleanliness Specification at the spacecraft magnetometer location when direct field measurements fail,

➢ and compensate the excess field.

➢ Reduce/eliminate the Magnetic Global Dipole Moment of a spacecraft so as to maximize the ACS life span of a spacecraft.

In order to achieve these tasks **GAMAG** extracts a numerical model of the magnetic potential of the test article in the form of a set of dipoles (Multiple Dipole Model, MDM).

This MDM allows then to calculate:

➢ the Global Dipole Moment of the test article.

➢ Field Vectors especially at locations where the Magnetic Cleanliness Specification has been written for Optimal Compensation Magnet Systems, for the compensation of the Global Spacecraft Dipole Moment and Field Vectors at Multiple Specification Points.

The **GAMAG** s/w package contains two versions:

➢ **GAMAG-B** for Field Measurements (used in low perturbing magnetic environment)

➢ **GAMAG-Bg** for Field Gradient Measurements (useful in strong perturbation environment)

In addition to these capabilities the **GAMAG** s/w package contains a number of simulation tools which are designed to assist a magnetic cleanliness program from the early design phases to launch.

➢ **BSIM** and **BgSIM**: MDM Field and Field Gradient Simulation

➢ **SSCM**: Synthetic Spacecraft MDM built-up from Unit MDMs (Fig.3)

➢ **DIMAL**: Dipole Moment Allocation List for cleanliness control. (Fig.4)

➢ **TSUCONF**: Optimal Test Set-Up Configuration for minimum MDM Ambiguity Errors (Fig.5)

➢ **TSUCAL**: Test Set-Up Calibration (Fig.6)

2.   Historical Background

During his 32 years of service in the European Space Agency ESA-ESTEC the author pioneered many facets of Magnetic Cleanliness for spacecraft. In 1977 he had introduced the so-called Multiple Magnetic Dipole Modelling Method (MDM) for spacecraft. Since then the method was applied successfully for many international scientific projects and it is presently the most used approach at ESA and European industry and institutes.

The most famous spacecraft were:
- GEOS (1980, ESA)
- ISEE-B (1982, ESA)
- Giotto (1985, ESA)
- Ulysses (1986, ESA)
- Ulysses-RTG (1986, JPL)
- TSS 1&2 (1992, Italy, USA): COI FGM, magnetic test at MFSA/IABG, detailed magnetic cleanliness survey of the Space Shuttle bay at KSC
- CLUSTER I/II (2002, ESA)
- Cassini-RTG (2000, JPL)
- Huyghens (2002, ESA
- Rosetta (ESA)

In addition, countless unit modelling sessions were performed and so-called synthetic spacecraft MDMs were assembled for the prediction of the spacecraft cleanliness level. Alone for Cluster I and II they were about 500 unit MDMs generated.

The greatest success in magnetic cleanliness, achieved by use of the precursor version of **GAMAG**, was achieved in the case of the unique Ulysses spacecraft (Fig.1) which orbits the Sun at high latitudes. Despite very strong magnetic units on board like TWTs, experiments and a RTG, it is, thanks to precise MDMs and optimal compensation magnets, to date the magnetically cleanest spacecraft ever flown *).
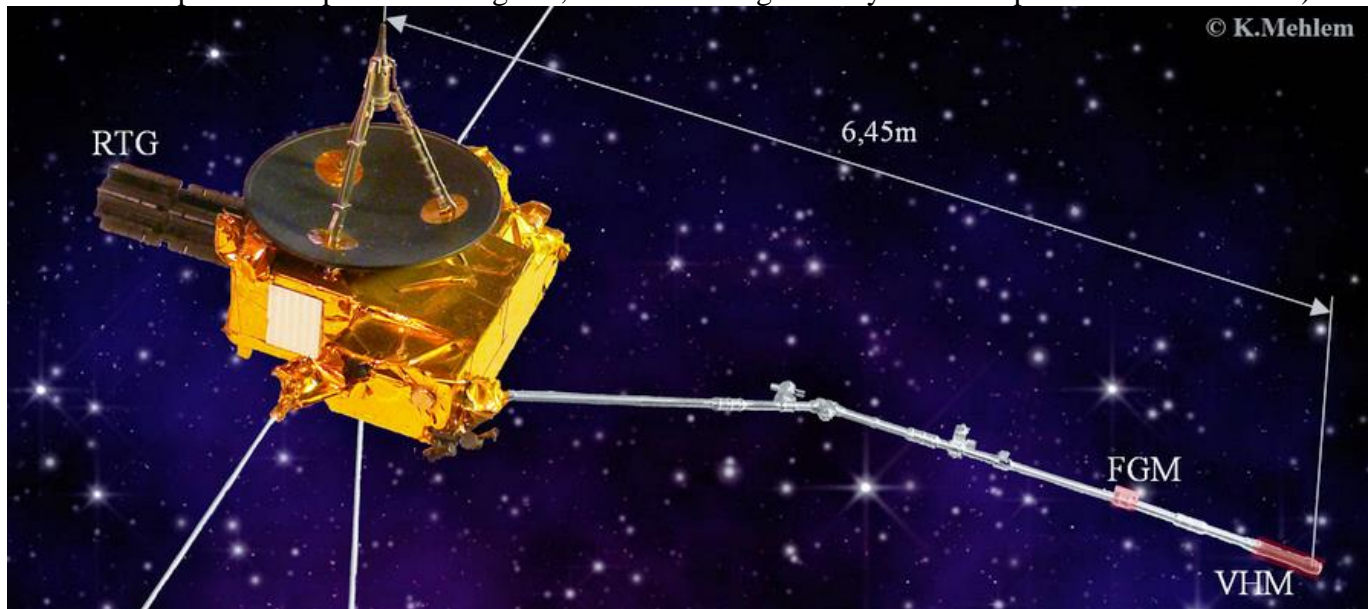
Fig.1 Ulysses in flight configuration

*) In: **The magnetic field investigation on the Ulysses mission: Instrumentation and preliminary scientific results**

A. Balogh[1], T.J. Beek[1], R.J. Forsyth[1], P.C. Hedgecock[1]*, R.J. Marquedant[2], E.J. Smith[2], D.J. Southwood[1] and B.T. Tsurutani[2]

Quote: "…Using magnetic mapping and modelling and appropriate compensation, the background field of the spacecraft at these locations was determined, prior to launch, to be approximately 30 pT and 50 pT, respectively. … Both magnetic mapping and modelling indicate the unparalleled cleanliness of the spacecraft, confirmed in flight."

The author retired from ESA in 2004 as a specialist in magnetic cleanliness of spacecraft. However, at the time of his retirement the operation of the software was still requiring an expert user. This was caused by a number of unresolved numerical problems, some related to the sparsity of input data, leading to MDM solution ambiguities, others to typical NLP issues like initial guess generation, parameter constraints, Jacobian matrix rank-control, convergence speed and robustness etc.

For this he has invested more than 4000 hours for the development of the much more powerful **GAMAG** s/w with the goal to create a high precision, fast and automatic state-of-the-art tool for magnetic cleanliness determination and improvement, suited to be used on-line as integrated tool in any coil facility, and of course in stand-alone mode.

The author presently continues as collaborator of Astos Solutions GmbH in Stuttgart, Germany, to develop methods and s/w for magnetic cleanliness.

3.   Elements of Realization

3.1. Data Acquisition

Magnetic Cleanliness Verification is based mainly on near-field measurements around a unit or a spacecraft and at a suitable distance.
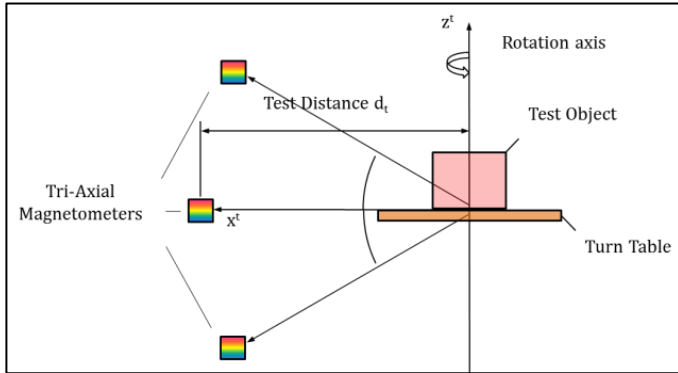
From these field measurements the **GAMAG** software extracts the magnetic potential of the test article in form of a Multiple Dipole Model (MDM)

Fig.2 Test Setup

Examples for a Small Coil Facility (SCF) and of a Large Coil Facility (LCF) are given in the Figures 3 and 4, respectively.
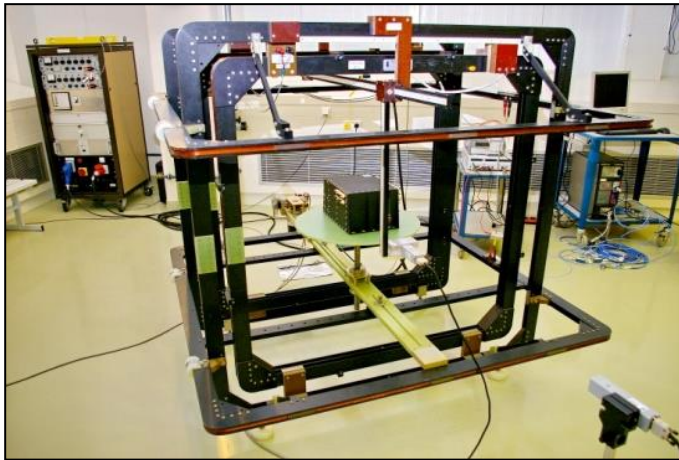
Fig.3 Small Coil Facility (1.6m) (Curtesy ESTEC, NL)   Fig.4 Large Coil Facility (12m) (Curtesy IABG, D)
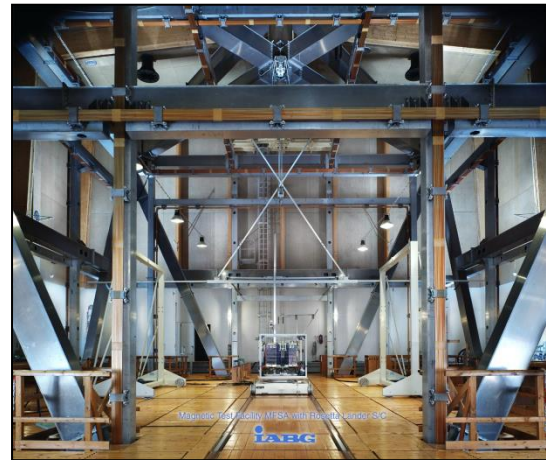
Rotational   Translational   Static
                                       and Pendulum
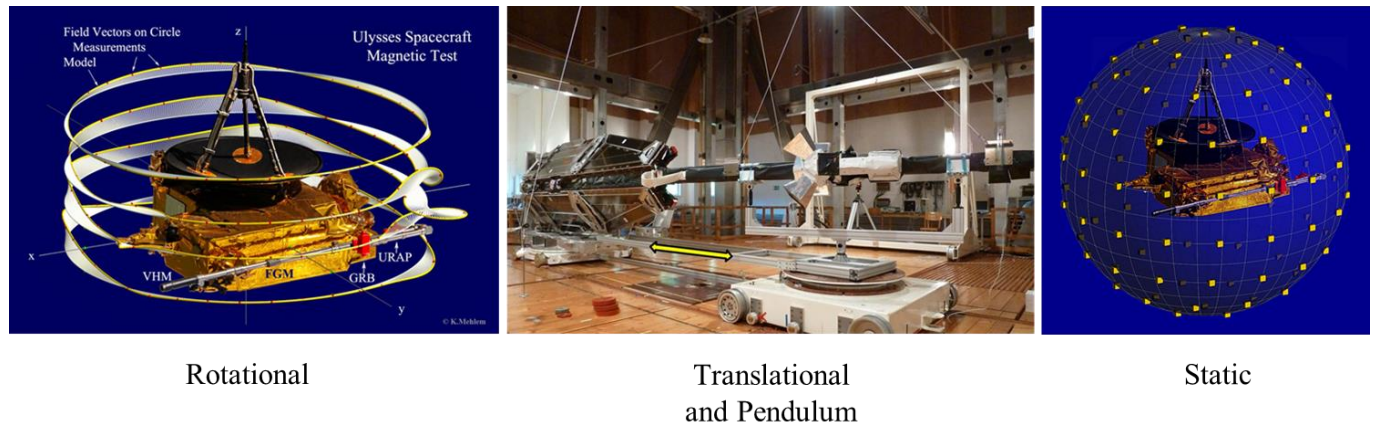
Fig.5 GAMAG Data Acquisition Modes

The data acquisition modes enabled in GAMAG are depicted in Fig.5.

A spacecraft ready for rotational data acquisition mode is shown in Fig.6. The spacecraft sits on a non-magnetic trolley which is fixed on the turntable. Four magnetometers are mounted next to the spacecraft. The magnetic states in which the spacecraft is tested are:
- Incoming
- Demagnetized
- Magnetized
- Demagnetized
- Compensated

For all states MDM's are extracted by **GAMAG** and the associated fields at the spacecraft magnetometer are calculated. From the last Demagnetized state the compensation magnets are determined, produced and fixed on a free place on the spacecraft, and the total is measured again. A final MDM is extracted which reveals the achieved compensation effect.

Fig.6 A Spacecraft in the Large Coil Facility of IABG, Munic, Germany

3.2. <u>Concept of the MDM Method</u>
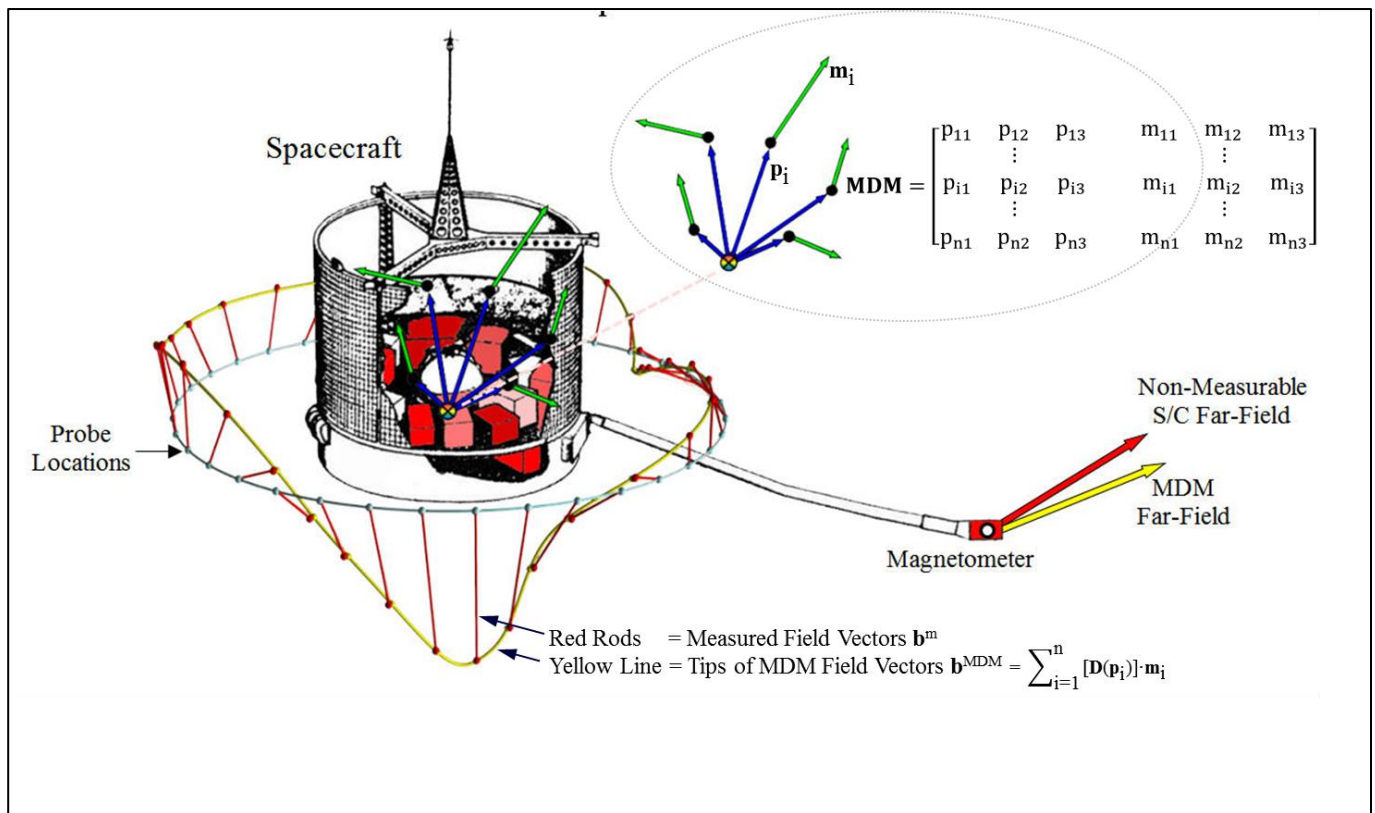
Fig.7 Concept of the MDM Method

<u>Case 1</u>

For a scientific spacecraft a spacecraft magnetometer is located at the tip of a boom. The cleanliness specification at this location is typically a fraction of 1 nT. Unfortunately, this field level is below the resolution of even the best coil facility. By consequence, the cleanliness specifcation can not be verified by direct field measurements. The solution of the problem is obtained by adding an intemediate step. It consists in collecting field measurements at closer distances where the signal to noise ration is much higher than at the magnetometer location. Frome these field measurements an optimal MDM (see explanation below and on Fig.7) can be found which allows to predict the field at the magnetometer location with high precision. Also, if the specification is exceeded, a compensation magnet can be determined which compensates the field at the magnetometer location to very low strengths.

<u>Case 2</u>

For a spacecraft in LEO its magnetic dipole moment by interaction with the geomagnetic field generates a torque on the spacecraft which has to be counterbalanced by the Attitude Control System (ACS). For a 3-axis stabilized spacecraft using cold gas thrusters this torque translates directly into the fuel consumption and hence into the life span of the mission. For the design of the ACS and for the maximization of the life span it is therefore paramount to know exactly the strenth of the spacecraft dipole moment, in order to define a compensation magnet which eliminates a large portion of that moment.

3.3. <u>MDM Determination</u>

The method is based on the postulate that any magnetic object can be represented by a number of magnetic dipoles.

A spacecraft, as depicted in Fig.7 contains a number of more or less magnetic units. A series of associated field vectors (red bars) are measured in steps of 10 deg one or more circles.

The task is then to find the necessary number of dipoles, their position vectors $\mathbf{p}_i$ and their moment vectors $\mathbf{m}_i$ which explain the measured field vectors in the sense of a least square fit. These parameters form the MDM.

3.3.1. <u>MDM Parameter Identification</u>

For a suitable number of dipoles the optimal positions $\mathbf{p}_i$ are found by use of a NLP solver of type Gauss-Newton which, starting from an initial guess (see Fig.8), improves the data fit iteratively until the desired fit precision is reached (see Fig.7). Since the moments are a linear function of the field measurements the optimal moments $\mathbf{m}_i$ can be founmd directly by the pseudo-inverse of a matrix.
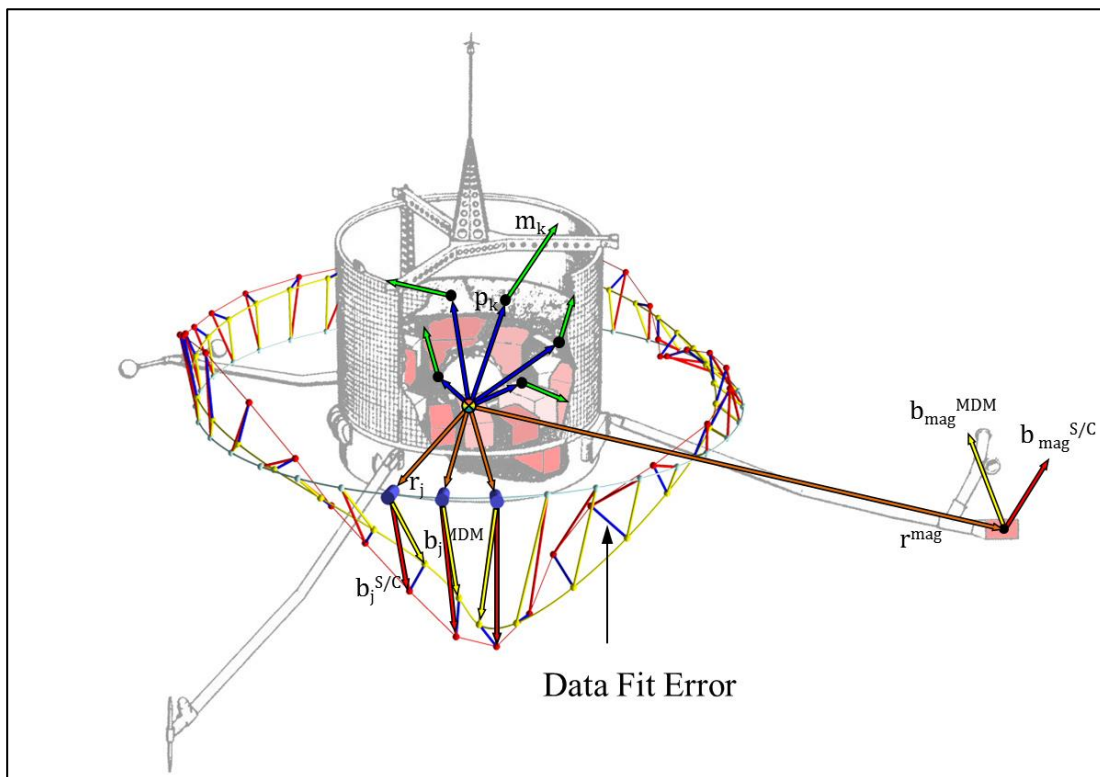
Fig.8 Initial parameter guess, leading to a bad data fit.

Once the data fit errors are minimized the associated optimal MDM allows then to calculated the field at the magnetometer location (Case 1) or to derive the global moment of the spacecraft (Case 2).

3.3.2. <u>MDM Solution Ambiguities</u>

A magnetic potential can only be described by a unique MDM solution if the latter is based on an infinity of measurement points on a closed surface around the test aricle, for instance on a sphere.

In practice this is of course not feasible. Due to the data gaps in which no information exists, there is a host of possible MDM solutions which all produce the same least square fit at the data points, but which show considerable deviations (ambiguities) within the data gaps (see Fig.14).

In Fig.9 the Ambiguity Error is defined.
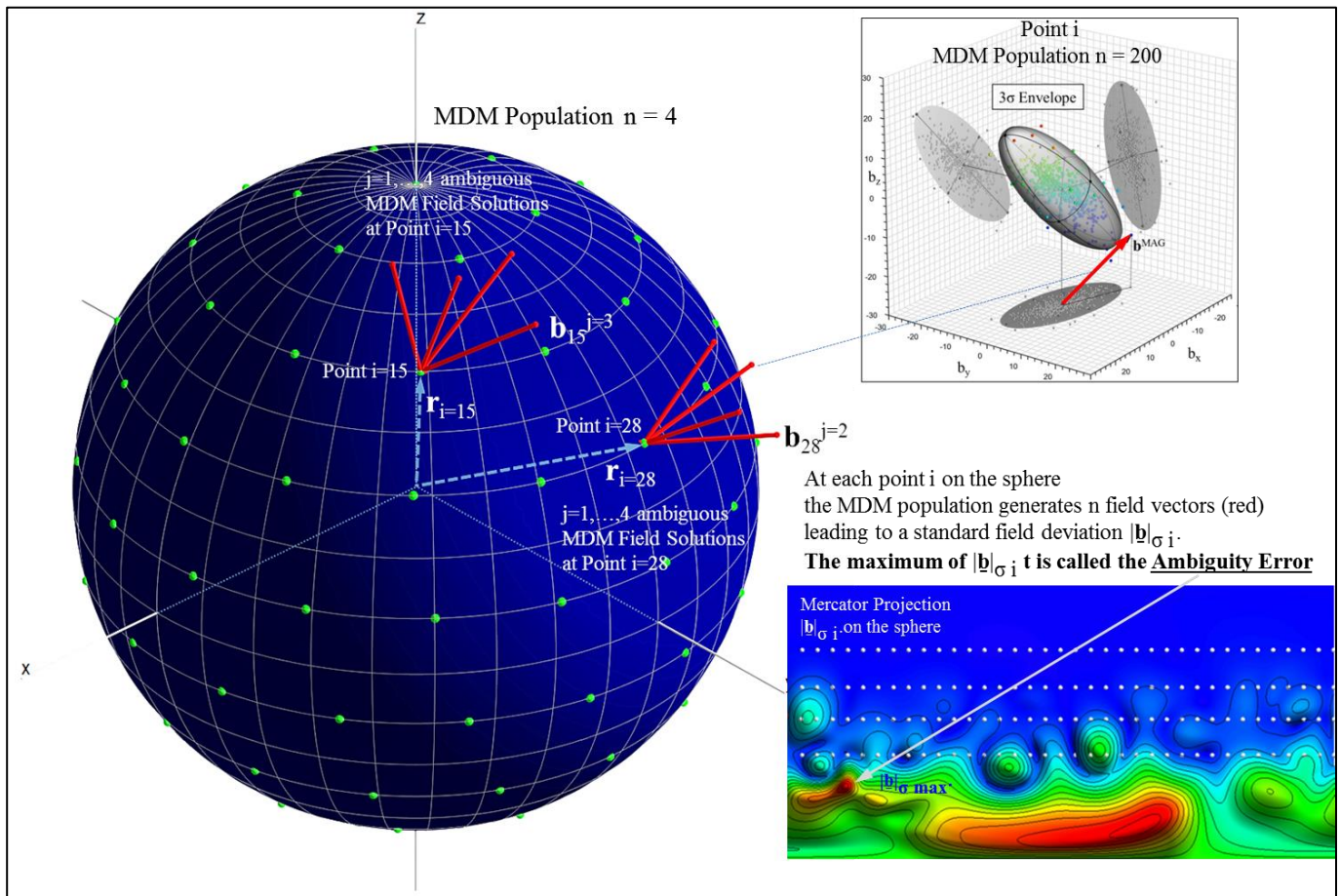
Fig.9 Definition of the ambiguity error

The 3σ deviations inside a population of optimal MDM solutions, as shown on Fig.10, are inceasing from blue to red. The red dots are the measurement points. The influence of the data coverage is evident. The figure on the right contains as many data points as the one in the center; but the maximum of the deviations is much lower.
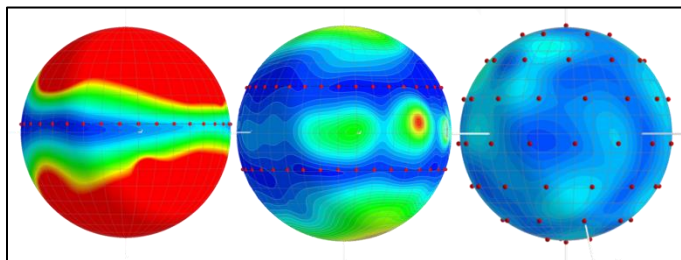
Fig.10 Ambiguity errors for differenet data coverage

A considerable part of the **GAMAG** software is dedicated to the statistical evaluation of the ambiguity errors on a centered sphere, in terms of their mean and 3σ deviation values. In particular, the <u>uncertainty</u> of the <u>field</u> at the magnetometer location and of the <u>global spacecraft moment</u> is calculated.

4. Examples
4.1. Example of GAMAG-B MDM Results

```
Legend:
=======
nd        = Number of Dipoles
C         = Cost Function
Stc       = Relative Cost Function              [%]
Stcmin    =  " Stagnation Stop Condition        [%]
Res       = Rms of Field Residues              [nT]
Res%      = Normalized Rms of Field Residues    [%]
Scf       = Self-Compensation Factor = Z|mi|/|Zmi| [-]
Wf        = Weighing Factor for Scf Term        [-]


MDM Optimization by nd-Increase:
==================================
 nd        C        Stc     StcMmin    Res      Res%     Res%min    Sfc        Wf
  1     16094.8    4.322    0.021     6.104    58.546    1.500    1.000 0.200D+00
  2      7414.1    1.961    0.021     4.143    39.735    1.500    1.114 0.200D+00
  3      2993.3    1.541    0.021     2.601    24.952    1.500   14.969 0.200D+00
  4      2394.6    0.271    0.021     2.330    22.353    1.500   12.243 0.200D+00
  5      2035.4    0.186    0.021     2.144    20.565    1.500   12.114 0.200D+00
  6      1461.6    0.342    0.021     1.802    17.281    1.500   12.710 0.200D+00
  7      1202.3    0.174    0.021     1.628    15.611    1.500   12.226 0.200D+00
  8       988.5    0.155    0.021     1.473    14.128    1.500   11.220 0.200D+00
  9        78.0    1.077    0.021     0.396     3.796    1.500    3.620 0.200D+00
 10        31.9    0.164    0.021     0.232     2.225    1.500    2.907 0.200D+00
 11        27.6    0.023    0.021     0.209     2.000    1.500    2.860 0.200D+00
 12        21.2    0.030    0.021     0.178     1.711    1.500    2.519 0.200D+00
 13        20.9    0.002    0.021     0.176     1.691    1.500    2.520 0.200D+00
Stop Condition met      ===============
```

The Optimal Number of Dipoles = 13   Spacecraft I

```
====================================
           Position                         Moment              Radius   Moment    Scf
     px        py        pz         mx       my       mz         rxy      |m|
             [cm]                          [mAm^2]                [cm]    [mAm^2]    [-]
 1  126.2035   78.9161  254.9349   -208.2    132.7    263.9     148.8    361.4
 2  133.4689  -36.3706  191.3314     -9.6    -74.8   -437.0     138.3    443.5
 3   95.8408   67.0218  177.6751    577.3    318.1   -639.4     117.0    918.3
 4   71.9924 -127.2350  185.6102   -127.1   -253.2    -27.2     146.2    284.6
 5  -78.1370  -92.2089  253.8912    -12.2    -45.2   -110.0     120.9    119.6
 6 -128.1474  -77.0148  262.0289    172.1    -73.4    210.0     149.5    281.3
 7  -27.8527  127.0934  188.8471   -111.9    -18.9   -432.7     130.1    447.3
 8  -95.3469  -62.4145  174.6597   -481.5   -151.1   -181.1     114.0    536.1
 9  -59.6464  159.1926  236.7537     -3.3    -18.1      2.6     170.0     18.6
10  -92.3152   71.6453  171.5589   -371.8    -54.7    -13.4     116.9    376.1
11   26.1604  -93.8015  234.1340     48.0   -146.9    -54.0      97.4    163.7
12   67.7798   74.2249  272.2657     43.2    -27.4    -42.2     100.5     66.3
13  -73.4415   32.0608  322.1688     -1.6      0.0     -1.3      80.1      2.0

Global Moment =................    -486.6   -412.8  -1461.9       0.0    1595.0    2.52
=============
```

```
Check Compliance with Cylinder Constraints [cm]:
=================================================
                        r        z
upper constraint     170.00   380.00
highest value        170.00   322.17
lowest  value        170.00   171.56
lower constraint     170.00   100.00
```

```
Optimal MDM Characteristics:     Spacecraft I
============================
Rms of Field Measurements       BMrms  =  10.426   [nT]
Rms of Field Residues           Res    =   0.176   [nT]
Normalized Rms of Field Residues Resp  =   1.691   [%]  of BMrms
Self-Compensation Factor        Scf    =   2.520   [-]
Constraint Violation            Cv     =   0.000   [cm]
```

```
Field Residues per Probe:
==========================
             Total Res =  0.176 [nT], =   1.69 % of BMrms
   |        x        |        y        |        z        |
   |  Ri   Rpi  Rimax |  Ri   Rpi  Rimax |  Ri   Rpi  Rimax |
   | [nT]  [%]  [nT]  | [nT]  [%]  [nT]  | [nT]  [%]  [nT]  |
 1  0.160 1.54  0.45  0.180 1.73  0.42  0.195 1.87  0.42
 2  0.176 1.69  0.39  0.172 1.65  0.48  0.224 2.15  0.57
 3  0.152 1.46  0.29  0.170 1.63  0.44  0.216 2.07  0.42
 4  0.110 1.05  0.27  0.164 1.57  0.40  0.170 1.63  0.43
```

```
Generation of Ambiguous MDM Solutions
=======================================
   j   nd    Resj    Resm +- Res3s    Scf    Dmin    Mgj      Mgm  +- Mg3s    Bspj    Bspm +- Bsp3s    STCR    STCRlim

   1   13   0.176   0.176   0.000    2.5     0.0  1595.0     0.0     0.0  1.2090  0.0000  0.0000  0.0000  2.0000
   2   13   0.181   0.179   0.007    2.5   392.2  1599.0  1597.0     5.9  1.2095  1.2093  0.0007  0.0000  2.0000
   3   13   0.180   0.179   0.006    2.6   239.4  1604.1  1599.4    11.1  1.2142  1.2109  0.0070  0.0000  2.0000
   4   13   0.169   0.177   0.014    2.3   237.4  1602.4  1600.1    10.4  1.2124  1.2113  0.0064  0.0000  2.0000
   5   13   0.175   0.176   0.013    2.4    47.9  1600.3  1600.2     9.3  1.2112  1.2113  0.0057  0.0000  2.0000
   6   13   0.173   0.176   0.012    2.5   136.1  1612.3  1602.2    16.0  1.2161  1.2121  0.0075  0.0000  2.0000
   7   13   0.213   0.181   0.040    2.7   193.4  1633.3  1606.6    35.9  1.2248  1.2139  0.0150  0.7447  2.0000


Data Coverage on the Sphere (r = mean measurement distance)
===========================================================
Homogeneity of Probe Distribution H          =    0.26601
Density      of Probe Distribution D          =    0.00348
Coverage Index  C=H*D                         =    0.00093


Error Budget:
=============
Field Data Truncation Error          Etr    =   0.025 [nT]
Estimated Signal-to-Noise Ratio      SNR    >    33.8 [dB]
Mean Field Fit Error (np=144,nd=14)  Resm   =   0.181 [nT]
Non-reductible Rest Error (Noise etc.) Erest ~   0.181 [nT]

Mean Global Moment                   Mgm    = 1600.3 [mAm²]
Global Moment at 3 Sigma             Mgm+3s = 1642.5 [mAm²]

Mean Field at Obs.Point              Bspm   =   1.211 [nT]
Field at Obs.Point at 3 Sigma        Bspm+3s =  1.229 [nT]

Mean MDM Ambiguity Error =B3sm   Sph.1  Em1    =   1.228 [nT]
Max. MDM Ambiguity Error =B3smax Sph.1  Emax1  =   4.264 [nT]

Mean MDM Ambiguity Error =B3sm   Sph.2  Em2    =   0.058 [nT]
Max. MDM Ambiguity Error =B3smax Sph.2  Emax2  =   0.111 [nT]
```

In the table above a typical **GAMAG** result is shown. In the first part the minimum necessary number of dipoles is determined (here n=13) and in the second part the results of the statistical analysis is reported (red mean/3σ value; spacecraft momemt = 1600.3/1642.5 mAm²; field at the specification point = 1.21611/1.229 nT). The ambiguity error on sphere 1 is shown on Fig.10b. Note the coverage problem.

The mean values are then used to define a magnet whether for the moment compensation of the spacecraft (ACS issue) or for the field compensation at the specification point (magnetometry mission).
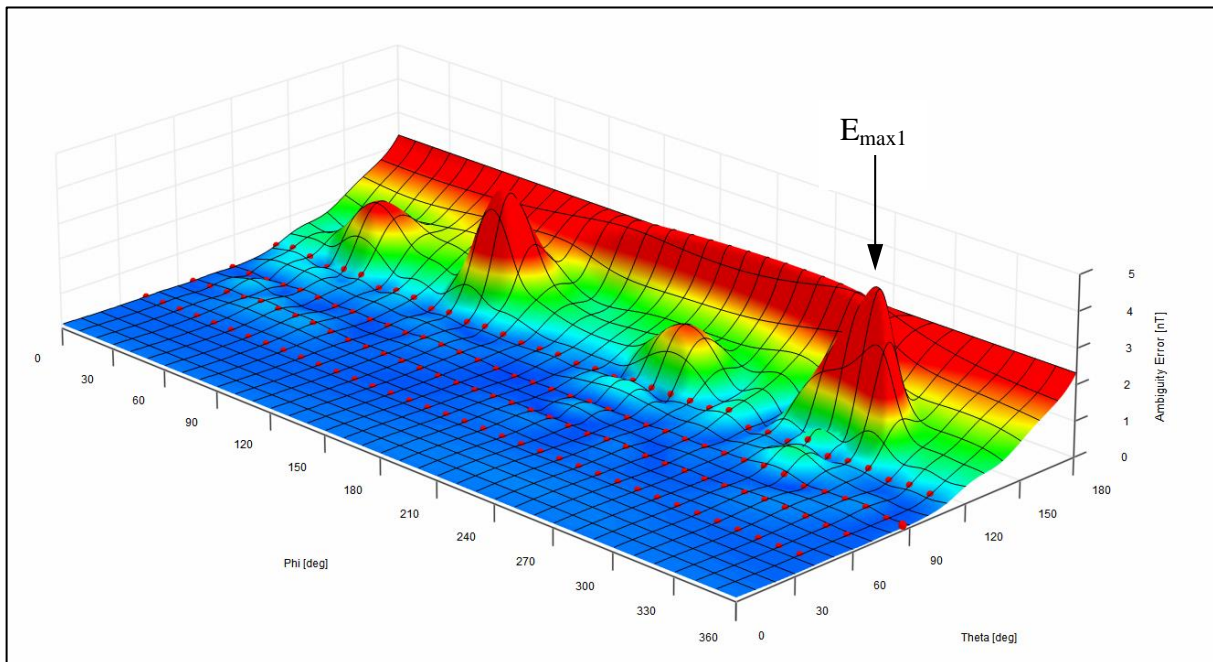
Fig.10b Mercator projection of the ambiguity error on a centered sphere (r = measurement distance)
(red dots = measurement points where the ambiguities are reduced by LSF)

4.2. **Example of GAMAG-B Field Compensation Results**

```
Compensation Point Coordinates:
================================
       px         py         pz
                 [cm]
1     404.9       -0.3      281.2
2     604.9       -0.3      281.2
3     604.9       -0.3      281.2


Field at Compensation Points before Compensation:
==================================================
       bx         by         bz       |b|
                 [nT]
1 -5.1340    -0.3323     2.3112     5.6401
2 -0.9382    -0.0076     0.7660     1.2112


Optimal Compensation Magnets in Cartesian Coordinates:
========================================================
            Position                     Moment
      px         py         pz         mx         my         mz      |
                 [cm]                             [mAm^2]
1   113.2000   -6.2000   266.4000      639.5    -1222.2    -5966.7
2   103.5000   -9.8000   260.7000     -263.8     1308.8     7354.8


Global Magnet Moment:                    375.6       86.6     1388.1     144
=====================


Compensation Magnet Box Constraints:
=====================================
            x          y          z
                     [cm]
min      90.00     -20.00     245.00
max     150.00       0.00     270.00


Optimal Compensation Magnets in Polar Coordinates:
====================================================
            Position            Moment      Phi       Theta
            [cm]                [mAm^2]     [deg]      [deg]
1   113.2000   -6.2000   266.4000    6124.0     -62.4      167.0
2   103.5000   -9.8000   260.7000    7475.0     101.4       10.3


Field at Compensation Points after Compensation:
==================================================
       bx         by         bz       |b|      Reduction
                 [nT]                            Factor
1  0.0000     0.0000     0.0000     0.0000       999.9
2  0.0000     0.0000     0.0000     0.0000       999.9
```


Fields before Compensation
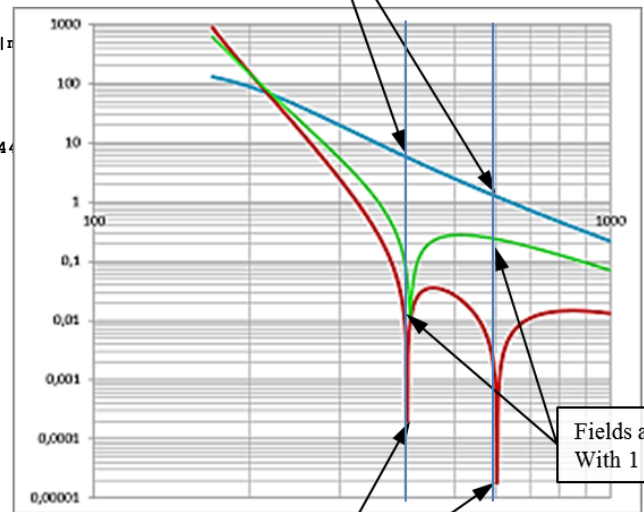
Fields after Con
With 1 Magnet

Fields after Compensation
With 2 Magnets

In the table above a dual-point field compensation with two magnets is demonstrated. Departing from 5.6401 nT at the inboard magnetometer and from 1.2112 nT at the outboard magnetometer the two optimal compensation magnets produce numerically exact zero fields at both locations (red curve).

With the add-on tools in the **GAMAG** package it is possible to estimate very accurately any achievable compensation.

The green curve shows what can be achieved with a single magnet for the dual-point compensation. A suitable weighing factor would lead to a more equilibrated solution.

GAMAG allows also to optimize the locations of the magnet. In principle it is possible to generate two zero fields with only one magnet. In general, **GAMAG** allows a host of combinations of numbers, locations, moments etc. which are equivalent to the original MDM identification possibilities.

4.3.   Spacecraft Dipole Moment Compensation
4.3.1.   Introduction

The torque acting on a spacecraft by interaction of its magnetic dipole moment with the geomagnetic environment is by far the predominant disturbance torque at altitudes below 1500 km. A typical geomagnetic field strength at 200 km is around $3*10^4$ nT. In this environment a 3-axis stabilized spacecraft with a dipole moment of 1 Am^2 would be disturbed by a torque of about $3*10^{-5}$ Nm. The energy wasted by fighting the geomagnetic disturbing torques is linearly dependent on the spacecraft magnetic dipole strength.

Other disturbing torques (radiation from the sun, gravity gradient, aerodynamics etc.) would be of an order of magnitude weaker.

4.3.2.   Spacecraft MDM obtained by System Test in a Large Coil Facility

The realism of the study results has been pushed to the limits of feasibility by use of the following steps:

1. A Multiple Dipole Model (MDM) of a real and representative spacecraft of medium size was chosen (Table 1). It had previously been extracted with very high precision from real rotational field measurements by using the GAMAG_B software.
2. The global dipole moment of the MDM was determined.
3. The MDM was then augmented by a theoretical compensation dipole moment vector, equal to the global moment vector but with opposite sign and located at a feasible place on the spacecraft; hence the overall global moment of the augmented MDM was zero (Table 1).
4. Realistic field measurements were then simulated by use of the BSIM software; the inputs were:
    a. The augmented MDM (Table 1).
    b. A realistic number of 7 tri-axial probes distributed equally on a half-circle at 280 cm distance.
    c. Typical normal distributed measurement noise of 0.3 nT.
    d. Conservative probe misalignments of 1 deg.
    e. Typical rotational step size of 10 deg.
5. Like in a real system test of a spacecraft these measurements, representing the spacecraft with the compensation magnet, were used to extract a new and independent MDM (GAMAG_B).
6. Since there is no unique MDM solution due to the relatively low number of measurements available a population of 20 ambiguous MDM solutions was generated and a statistical evaluation was performed leading to the mean and 3σ values of the global moment norm.
7. In order to check the worst case compensation effect the severe 3σ value of the global moment norm (Point 6) was compared to the global moment norm of Point 1.

MDM of a Real Spacecraft + Moment Compensation Magnet							
p_x	p_y	p_z	m_x	m_y	m_z	|m|	
[cm]			[mAm^2]				
128,56	80,30	255,29	-182,40	120,30	218,30		
-30,27	135,67	190,51	-55,30	-51,20	-373,30		
131,82	-33,11	192,53	-33,60	-80,40	-464,40		
-127,07	-77,30	261,18	180,90	-68,70	220,90		
-81,64	-92,28	252,57	-55,50	-41,90	-117,30		
-98,09	-64,33	180,09	-433,10	-118,20	-257,80		
13,99	-98,51	235,62	-37,30	-129,50	-35,80		
66,72	68,91	277,25	94,30	-4,40	-26,30		
-89,67	69,28	171,61	-398,80	-20,90	-7,20		
51,23	82,52	334,73	-2,20	-1,70	2,20		
63,49	-129,94	178,17	-38,80	-248,90	4,60		
97,42	70,27	178,75	506,90	248,70	-643,90		
100,50	-128,85	224,95	-33,90	-18,80	13,90		
113,20	-6,20	266,40	488,80	415,60	1466,10	1600,34	Ideal Moment Compensation Magnet
Global Moment			0,00	0,00	0,00	0,00	

Table 1 Original spacecraft MDM (**Torque = $4.80*10^{-5}$ Nm**) augmented by the compensation magnet

Particular MDM Solution of Compensated Spacecraft by Reverse Engineering						
p_x	p_y	p_z	m_x	m_y	m_z	|m|
[cm]			[mAm^2]			
116,83	-5,82	25,03	277,00	480,80	1539,80	
128,84	-35,65	-53,72	87,40	-70,40	-379,50	
-73,36	-77,68	1,83	-1085,80	-290,10	1097,10	
-114,14	-69,96	-29,24	248,40	38,20	-949,50	
-31,16	136,96	-48,47	-13,80	-40,70	-343,00	
60,47	-124,01	-55,98	-30,50	-339,10	-11,10	
109,07	78,49	-47,92	-81,50	-95,00	-1055,40	
-88,76	63,63	-67,31	-404,20	69,40	16,70	
85,47	83,24	-17,04	652,60	292,70	385,10	
-46,73	-98,28	13,14	427,30	-100,30	-386,30	
143,15	79,92	35,43	-72,30	47,00	74,90	
103,46	-134,89	-25,85	-21,30	-2,10	13,40	
Global Moment			-16,70	-9,60	2,20	19,39	Rest Moment after Compensation

19,50	Mean
24,70	Mean + 3σ

98,46	Moment Reduction Factor at 3σ [%]

Table 2 A realistic MDM solution with a rest global moment (**Torque = 7.41*10^{-7} Nm**), taking onto account the above cited disturbances.

The main result, supported by extensive experience with even complex spacecraft at ESA, is that by use of the **GAMAG** software a reduction of the global dipole moment of $> 95\%$ appears to be feasible.

In the present case study, despite the conservative approach, the magnetic torque is comparable to all other perturbation torques. The increase of life span is estimated to be well over 10% per a nominal life span and the derivative of the increase of live span w.r.t. to the increase of the compensation factor has been found to be directly proportional.

Please note that this result is based on the assumption that magnetic cleanliness practices are applied like avoidance of soft-magnetic material which is the most important issue, of twisted harnesses and avoidance of other current loops etc.

Please note also that the GAMAG software is also capable of determining systems of compensation magnets for multiple-point field compensation (at multiple magnetometer locations) together with the suppression of the global spacecraft moment. This seems contradictory but the fact is that a spacecraft with a compensation magnet for the global spacecraft moment generates in general at medium distances higher order fields which decay rapidly with distance and which can simultaneously be fine-compensated at specific points.

4.3.3. <u>Synthetic Spacecraft MDM obtained from Unit Tests in a Small Coil Facility</u>

When a large coil facility (LCF) for a system test is not available the spacecraft MDM can be estimated via a Synthetic Spacecraft Model by use of an SCF and of the SSCM software.

For this all magnetic units have to be measured individually in a SCF and their MDMs and their ambiguity deviations (3σ) have to be extracted from the field data by use of the GAMA_B software.

If we assume

1. that the unit measurements are done with a maximum feasible coverage by 3 magnetometers, equally distributed on a half-circle at a signal-dependent optimal distance in order to minimize the ambiguity deviations,
2. that the units contain at most a negligible amount of soft-magnetic materials,
3. that the environmental noise is kept to about 1-2 nT,
4. that the unit MDM and its ambiguity deviation is extracted with the maximum feasible accuracy (GAMAG_B software),

the precision of the results with respect to a system test would, due to accumulation of modeling errors, degrade at most by 10-15%, as experience shows.

4.3.4. <u>Synthetic Spacecraft MDM obtained without the Use of a Coil System</u>

When even a SCF is not available it is conceivable (however recommended only in emergency cases)

1. to derive the global moments of the most culprit units by use of a hand-held sniff-magnetometer, requiring certain skills,
2. to estimate the accuracy of the global unit moments by use of repetitive measurements at different distances,
3. to build-up a Synthetic Spacecraft Model from the most predominant culprit units, taking into account the uncertainty of the individual global unit moments,
4. to derive the global moment of the spacecraft together with its accumulated uncertainties,
5. to compensate numerically the global moment with a magnet of maximum likelihood,
6. to derive an estimate of the increase of life span.

In this case the achievable compensation factor will decrease again, but this time by a more substantial amount. The reduction of the spacecraft dipole moment has a favorable impact w.r.t. the ACS design and w.r.t. the life span of a spacecraft:

If a spacecraft is 3-axis stabilized by use of magnetic torquers their mass can be reduced according to the achieved compensation effect. In the favorable case (compensation > 95%) the torquers, if not used for other pointing requirements, can even be eliminated and their mass can be translated into fuel for the ACS. This can lead to a <u>considerable increase of the life span</u> of the ACS and thereby of the mission.

If a spacecraft is 3-axis stabilized by cold gas thrusters the same effect on life span is to be expected. When applying conservative assumptions the lower bound of the relative gain of life span has been estimated to around 18% of the nominal life span.

Please note that the present study demonstrates again the capability of the **GAMAG** toolbox to make realistic simulations and predictions (BSIM, DIMAL and SSCM software) without the need for a coil facility and for real field measurements.

4.4. GAMAG-Bg software

The **GAMAG** software has also been adapted to accept field gradient data as input.
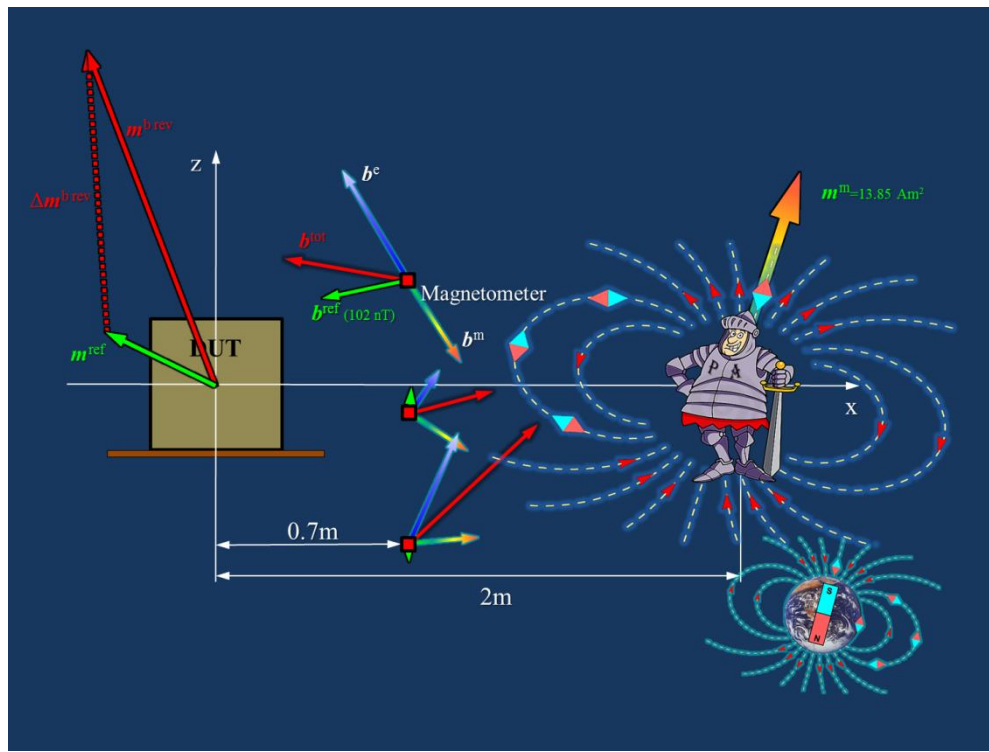
The output structure is identical to the one of field data. The field gradient has the important property to ignore all external perturbing fields which are constant over the length of a gradiometer sensor element. This fact can under certain precautions even be used when the magnetic tests have to be done without the help of a coil facility. Fig.11 illustrates the large modeling error Δm induced by external field perturbations like the indesirable presence of a PA guy is inducing.

Fig.11 Magnetometers: Influence of external pertirbations on the MDM accuracy
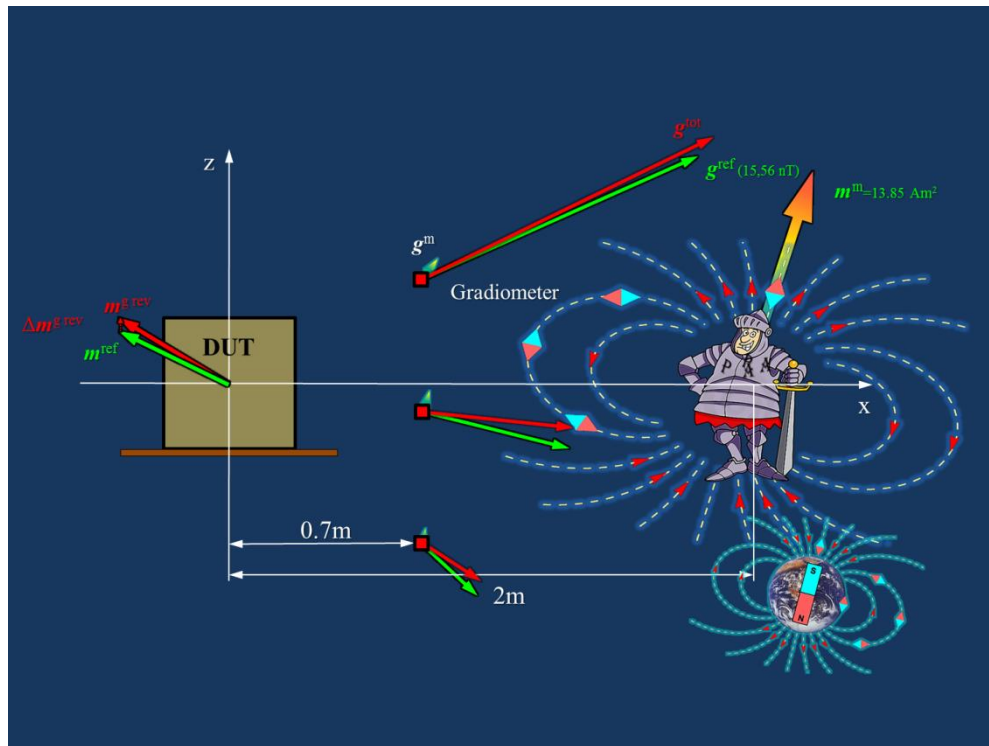
By using field gradient measurements instead (Fig.12, arrows not in the same scale as above) the reduction of the MDM error Δm by factor 18.8 is quite remarkable. But it has to be kept in mind that the gradiometer signal has decreased by factor 6.8 w.r.t. the magnetometer. Therefore a smaller measurement distance would be required.

Fig.12 Gradiometers: Increase of the MDM accuracy

In the following a MDM extraction has been performed on the basis of simulated gradiometer data (Fig.13):

1. The original unit MDM was augmented by a perturber dipole at 2 m distance generating 200 nT at the measurement point, and by a second perturber dipole at 100 m distance generating random ± 100 nT .

2. Rotational pseudo-gradiometer measurement data were simulated (BGSIM s/w, red points lying on green ref curve).

3. A new unit MDM was extracted (GAMAG-Bg s/w, red curve fitting red points).

4. The original (green) and the new (red) unit MDMs are very close despite the massive field perturbations.
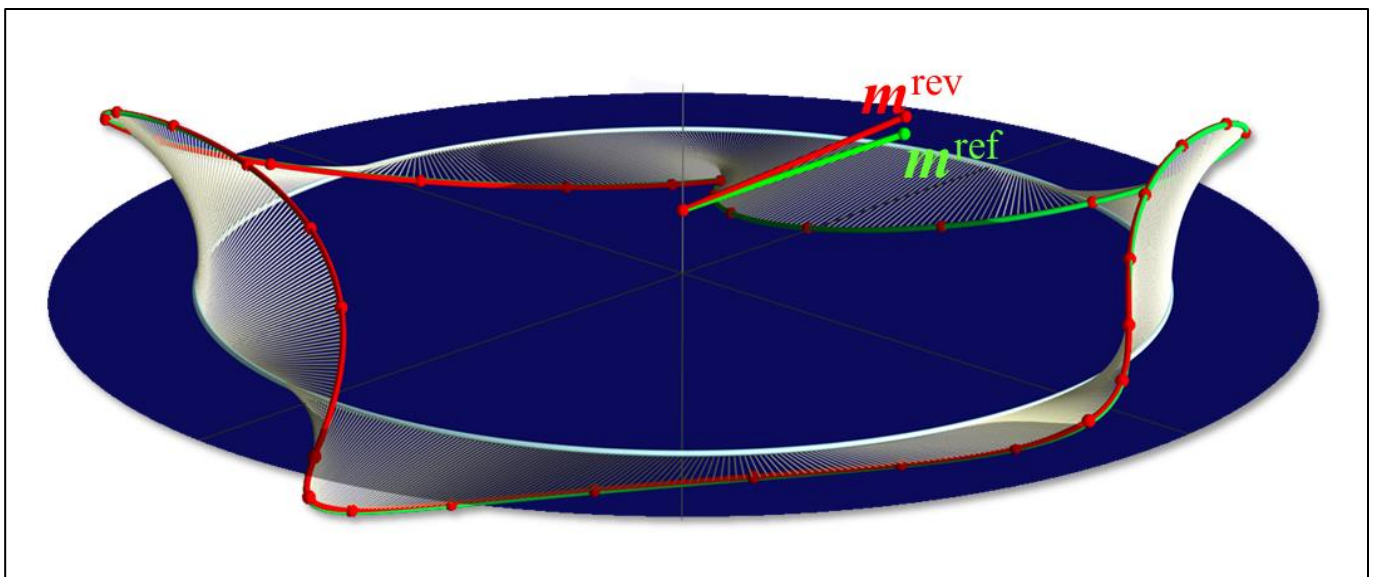
Fig.13 MDM extraction from gradiometer data in presence of strong perturbations

4.5. GAMAG-B/Bg Operational Robustness

An important improvement is also the robustness of the software w.r.t. differences in test configurations, test aricle magnetic characteristics, test facilitiy resolution etc. On Fig.14 is shown a table which contains 19 unit and 37 spacecraft test cases of the most challenging kind. These 58 test cases have been solved in a single batch run by use of the same optimization steering parameters and without any user intervention!

Definitions: Parameter Ranges

Inputs:

b_{rms}	= rms of field measurements [nT]	0,3 - 255,3
n_{pr}	= number of facility probes (rotational measurements, 10° step size)	1 - 72
r_m	= measurement distance [cm]	42 - 307,9
r_o	= radius of sphere through observation point [cm]	146,7 - 1096,2
r_c	= box constraint size [cm]	8,2 - 170
H	= homogeneity of data coverage	0,1 - 1
D	= density of data coverage	0,1 - 1
C	= data coverage index	0,0 - 1
n_{bmax}	= number of field maxima	1 - 8
SNR	= signal-to-noise ratio	2,1 - 92,6

Results: (green frame, blue frames contain good correlations between Scf and m_g)

n_d	= number of necessary dipoles	2 - 18
Res	= rms of field fit residues [nT]	0,1 - 12,4
Res%	= " as % of b_{rms}	0,2 - 43,1
Scf	= dipole moment self-compensation factor within a MDM	1,0 - 9,3
m_g	= global dipole moment [mAm²]	0,4 - 1652,6
$m_{g3\sigma}$	= 3σ deviation of m_g [mAm²]	0,0 - 15,1
b_o	= field at observation point [nT]	0,0 - 40,2
$b_{o3\sigma}$	= 3σ deviation of b_o [nT]	0,0 - 90,8
E_m	= MDM ambiguity error at measurement distance r_m [nT]	0,3 - 90,7
E_o	= MDM ambiguity error at observation distance r_o [nT]	0,0 - 3,5

	DUT	b_{rms}	n_{pr}	r_m	r_x	r_z	H	D	C	nb_{max}	SNR	n_d	Res	Res%	Scf	m_x	m_{yb}	b_x	b_{xb}	E_m	E_x	T(s)
1	Unit RPU	55,9	3	49,3	500,0	20,0	0,264	0,266	0,070	3	54,5	6	0,86	1,5	1,6	62,7	2,0	0,050	1,684	4,91	0,003	39,6
2	Unit Battery	178,9	1	50,0	400,2	13,2	0,089	0,089	0,008	2	28,3	4	4,73	2,6	3,7	264,7	12,6	0,546	10,794	22,49	0,034	4,1
3	Unit X	85,7	4	160,0	500,0	10,0	0,175	0,355	0,062	3	6,8	3	12,42	14,5	2,7	993,0	1,6	1,156	1,035	2,72	0,078	3,1
4	Unit FGU AR	8,4	3	51,3	200,0	20,0	0,266	0,266	0,071	1	36,5	4	0,21	2,5	1,1	10,8	0,5	0,262	0,451	3,29	0,017	26,9
5	Unit FGU, run 60,	0,8	3	51,3	500,0	20,0	0,266	0,266	0,071	3	4,5	2	0,16	21,4	1,0	0,9	0,9	0,001	1,443	10,50	0,002	5,6
6	Unit GCMS AR	87,6	3	110,0	1096,2	25,0	0,266	0,266	0,071	2	76,6	4	0,94	1,1	1,4	1074,5	0,2	0,111	0,327	0,75	0,000	15,4
7	Unit GCMS Compens	41,9	3	110,0	1096,2	25,0	0,266	0,266	0,071	4	34,0	7	1,11	2,7	9,3	103,0	2,1	0,010	2,410	18,10	0,004	45,2
8	Unit HPA TWTA EQM	252,9	3	51,3	500,0	20,0	0,266	0,266	0,071	4	49,3	5	4,58	1,8	3,9	186,0	1,0	0,257	0,428	3,11	0,001	50,2
9	Unit HPA TWTA AR	255,3	3	51,3	500,0	20,0	0,266	0,266	0,071	4	48,0	5	5,19	2,0	3,7	172,9	1,2	0,242	0,813	3,78	0,002	32,8
10	Unit PSU, Run 10,	2,8	3	51,3	200,0	20,0	0,266	0,266	0,071	1	15,4	3	0,17	5,9	1,0	3,7	1,0	0,084	0,683	4,12	0,030	9,0
11	Unit PSU FD	0,3	3	51,3	200,0	20,0	0,266	0,266	0,071	8	2,1	6	0,15	43,1	1,3	0,4	11,6	0,006	5,253	49,07	0,300	24,5
12	Unit RTG compensated	5,7	3	150,0	779,9	70,0	0,239	0,266	0,064	4	16,9	10	0,32	5,6	3,5	91,9	6,6	0,018	6,101	30,71	0,063	89,5
13	Unit RTG	8,9	3	150,0	779,9	70,0	0,239	0,266	0,064	2	19,7	6	0,41	4,6	1,5	331,3	1,7	0,071	1,438	6,98	0,017	30,7
14	Unit Flywheel	73,8	3	54,6	300,2	20,0	0,264	0,266	0,070	1	6,7	3	7,10	9,6	4,8	108,3	14,5	0,428	13,786	19,45	0,125	3,7
15	Unit TWT	94,2	3	83,8	500,0	30,0	0,264	0,266	0,070	2	38,6	3	1,07	1,1	1,1	677,1	0,6	0,515	0,600	1,80	0,004	6,0
16	Unit Y	17,4	1	42,0	600,7	8,2	0,089	0,089	0,008	2	9,3	3	1,47	8,4	1,1	12,7	6,1	0,012	6,958	16,45	0,003	1,5
17	Unit TWT SP42 d=10	68,9	2	101,1	146,7	14,5	0,172	0,177	0,031	2	92,6	5	0,68	1,0	1,8	889,9	3,0	40,151	5,033	5,10	1,470	9,8
18	Unit TWT_Static	73,3	72	100,1	146,7	14,5	1,000	1,000	1,000	4	77,7	5	0,12	0,2	1,8	873,9	0,0	38,929	0,034	0,27	0,028	13,0
19	Unit TWT42+TWT44+Magnet	91,9	2	101,1	146,7	44,5	0,172	0,177	0,031	2	83,3	7	0,97	1,1	3,5	925,7	0,7	1,425	90,776	6,51	1,146	28,2
20	Unit Torquer	10,4	3	153,1	250,0	50,0	0,261	0,266	0,069	1	10,3	4	0,25	2,4	1,3	342,5	1,0	2,900	1,770	5,88	0,529	8,7
21	Spacecraft 1_FM1_01_AR	7,5	4	307,8	606,3	170,0	0,266	0,355	0,094	4	17,5	13	0,32	4,3	2,5	765,2	6,0	0,733	2,402	21,75	1,250	430,6
22	Spacecraft 1_FM1_02_PE	6,8	4	307,8	606,3	170,0	0,266	0,355	0,094	5	15,0	10	0,37	5,5	3,1	594,8	7,0	0,094	26,678	30,59	1,637	226,8
23	Spacecraft 1_FM1_03_DP	6,3	4	307,8	606,3	170,0	0,266	0,355	0,094	4	14,6	10	0,34	5,4	2,6	688,9	1,1	0,623	2,345	27,65	1,300	203,2
24	Spacecraft 1_FM1_04_CO	6,8	4	307,8	606,3	170,0	0,266	0,355	0,094	5	13,6	13	0,36	5,3	3,4	543,1	6,0	0,146	21,978	34,56	1,567	284,2
25	Spacecraft 1_FM1_05_FD	6,9	4	307,8	606,3	170,0	0,266	0,355	0,094	5	13,6	12	0,40	5,8	3,3	556,9	9,7	0,150	21,232	28,83	1,758	233,6
26	Spacecraft 1_FM2_01_AR	3,2	4	307,9	606,3	170,0	0,266	0,355	0,094	5	6,2	13	0,37	11,6	2,7	441,4	10,5	0,188	13,890	69,77	2,781	305,5
27	Spacecraft 1_FM2_02_PE	3,6	4	307,9	606,3	170,0	0,266	0,355	0,094	4	11,6	18	0,28	7,7	2,2	494,6	6,1	0,180	10,249	51,16	2,088	643,3
28	Spacecraft 1_FM2_05_FD	3,4	4	307,9	606,3	170,0	0,266	0,355	0,094	4	7,8	16	0,33	9,7	2,7	440,8	15,0	0,160	14,327	74,54	3,543	483,1
29	Spacecraft 1_FM3_01_AR	5,8	4	307,7	606,3	170,0	0,266	0,355	0,094	5	11,4	11	0,27	4,6	1,8	997,7	1,2	0,583	1,075	10,90	0,377	270,7
30	Spacecraft 1_FM3_02_PE	6,4	4	307,7	606,3	170,0	0,266	0,355	0,094	4	16,3	12	0,32	5,0	2,4	864,0	5,9	0,147	8,442	20,59	1,257	323,3
31	Spacecraft 1_FM3_03_DP	6,5	4	307,7	606,3	170,0	0,266	0,355	0,094	3	14,5	11	0,32	4,9	2,1	883,5	4,6	0,153	6,444	27,59	1,171	230,8
32	Spacecraft 1_FM3_04_CO	6,5	4	307,7	606,3	170,0	0,266	0,355	0,094	4	19,0	11	0,27	4,2	2,1	869,1	3,2	0,138	9,444	10,89	0,602	237,8
33	Spacecraft 1_FM4_01_AR	6,3	4	307,7	606,3	170,0	0,266	0,355	0,094	5	14,5	17	0,32	5,1	2,0	1034,2	4,1	0,712	2,609	24,78	1,200	637,7
34	Spacecraft 1_FM4_02_PE	7,2	4	307,7	606,3	170,0	0,266	0,355	0,094	5	11,9	10	0,50	7,0	3,2	624,8	7,4	0,125	8,938	30,43	1,838	201,5
35	Spacecraft 1_FM4_03_DP	6,2	4	307,7	606,3	170,0	0,266	0,355	0,094	5	11,9	16	0,32	5,1	2,6	980,0	7,9	0,668	4,094	28,20	1,823	543,4
36	Spacecraft 1_FM4_04_CO	7,2	4	307,7	606,3	170,0	0,266	0,355	0,094	5	12,3	10	0,55	7,6	3,7	629,1	6,3	0,120	7,951	36,16	1,799	185,3
37	Spacecraft 1_FM5_01_AR	6,4	4	301,5	606,3	170,0	0,266	0,355	0,094	4	11,7	12	0,27	4,2	2,2	983,2	6,5	0,665	5,545	34,85	0,993	286,3
38	Spacecraft 1_FM5_02_PE	7,8	4	301,5	606,3	170,0	0,266	0,355	0,094	4	12,6	11	0,53	6,8	3,9	569,3	5,0	0,101	19,229	24,97	0,930	219,8
39	Spacecraft 1_FM5_05_FD	7,8	4	301,5	606,3	170,0	0,266	0,355	0,094	5	9,7	9	0,66	8,5	4,0	568,0	4,4	0,090	23,864	34,00	1,413	148,8
40	Spacecraft 1_FM5_04_CO	7,8	4	301,5	606,3	170,0	0,266	0,355	0,094	5	10,2	9	0,68	8,7	4,0	576,5	4,5	0,091	15,383	41,78	1,473	169,5
41	Spacecraft 1_FM6_01_AR	9,1	4	301,5	606,3	170,0	0,266	0,355	0,094	4	22,5	11	0,31	3,4	2,1	1433,2	1,6	0,926	0,793	13,41	0,492	309,0
42	Spacecraft 1_FM6_02_PE	10,0	4	301,5	606,3	170,0	0,266	0,355	0,094	4	7,7	12	0,51	5,1	3,9	769,4	9,8	0,235	17,414	46,36	2,576	293,5
43	Spacecraft 1_FM6_03_DP	9,0	4	301,5	606,3	170,0	0,266	0,355	0,094	4	6,8	9	0,37	4,1	2,5	1371,4	1,8	0,893	1,053	34,82	1,047	162,4
44	Spacecraft 1_FM6_04_CO	9,9	4	301,5	606,3	170,0	0,266	0,355	0,094	5	6,6	10	0,63	6,3	4,4	738,9	14,0	0,185	35,220	90,67	3,430	174,9
45	Spacecraft 1_FM7_01_AR	8,3	4	301,5	606,3	170,0	0,266	0,355	0,094	5	11,3	15	0,27	3,3	2,3	1180,4	1,2	0,771	1,867	27,57	1,103	459,6
46	Spacecraft 1_FM7_02_PE	9,3	4	301,5	606,3	170,0	0,266	0,355	0,094	5	8,0	10	0,80	8,6	5,5	678,3	6,9	0,094	18,989	78,96	2,629	193,5
47	Spacecraft 1_FM7_03_DP	8,3	4	301,5	606,3	170,0	0,266	0,355	0,094	5	8,4	15	0,25	3,1	2,5	1199,7	5,6	0,781	4,238	30,20	1,240	476,6
48	Spacecraft 1_FM7_04_CO	9,4	4	301,5	606,3	170,0	0,266	0,355	0,094	5	10,6	11	0,50	5,3	3,6	696,3	1,4	0,062	11,769	27,96	0,833	261,3
49	Spacecraft 1_FM8_01_AR	10,4	4	301,5	606,3	170,0	0,266	0,355	0,094	5	15,8	11	0,45	4,3	2,1	1652,6	3,2	1,242	0,663	16,68	0,714	270,9
50	Spacecraft 1_FM8_02_PE	12,4	4	301,5	606,3	170,0	0,266	0,355	0,094	5	6,8	10	0,53	4,3	4,2	862,3	15,1	0,058	59,111	69,22	3,234	203,6
51	Spacecraft 1_FM8_03_DP1	10,4	4	301,5	606,3	170,0	0,266	0,355	0,094	5	6,3	10	0,28	2,7	2,2	1611,2	9,9	1,217	7,032	51,93	1,962	197,3
52	Spacecraft 1_FM8_04_CO	12,5	4	301,5	606,3	170,0	0,266	0,355	0,094	5	14,2	10	0,73	5,8	4,5	860,9	10,6	0,151	51,478	47,83	3,363	209,9
53	Spacecraft 2 Incoming, Ru	4,9	4	212,2	630,1	150,0	0,350	0,355	0,124	6	17,6	9	0,25	5,2	1,9	267,4	3,0	0,086	4,116	17,31	0,194	141,0
54	Spacecraft 2 Incoming, Ru	1,8	4	259,9	630,1	150,0	0,355	0,355	0,126	4	9,5	8	0,17	9,7	1,4	211,3	4,4	0,065	7,694	24,65	0,463	69,2
55	Spacecraft 2 Final Deperm	4,8	4	212,2	630,1	150,0	0,350	0,355	0,124	5	11,2	9	0,30	6,3	2,5	191,9	4,6	0,052	11,024	36,14	0,416	92,0
56	Spacecraft 2 Final Deperm	1,8	4	259,9	630,1	150,0	0,355	0,355	0,126	3	7,3	8	0,21	11,8	1,7	175,8	14,2	0,041	20,103	44,60	1,460	65,5
57	Spacecraft 2 Initial Depe	4,7	4	212,2	630,1	150,0	0,350	0,355	0,124	4	12,8	9	0,27	5,8	2,4	189,9	1,9	0,056	13,772	45,40	0,445	118,3
58	Spacecraft 2 Initial Depe	1,8	4	259,9	630,1	150,0	0,355	0,355	0,126	4	9,3	10	0,17	9,8	1,9	188,0	9,6	0,053	16,787	35,53	1,069	119,2

Fig.14 **GAMAG** robustness test

The results are all as expected. Outside the green frame the parameters shown are exterior data and in the green frame are collected to optimization results.

Also, a spectacular increase of speed has been achieved. Whereas the precurser version **GAMAG**, for a complex case of 12 dipoles, required for the generation of one MDM solution about 20-30 minutes due to frequent user interventions, **GAMAG** solves the problem in 12 seconds in an autonomous way.

5. GAMAG Grphical User Interface (GUI)
5.1. GAMAG-B GUI Input Pages

The GUI of **GAMAG** is a standard and simple to use tool to import and change input data. On the first page (Fig.15) it can be seen that only data are imported which stem from a test facility.
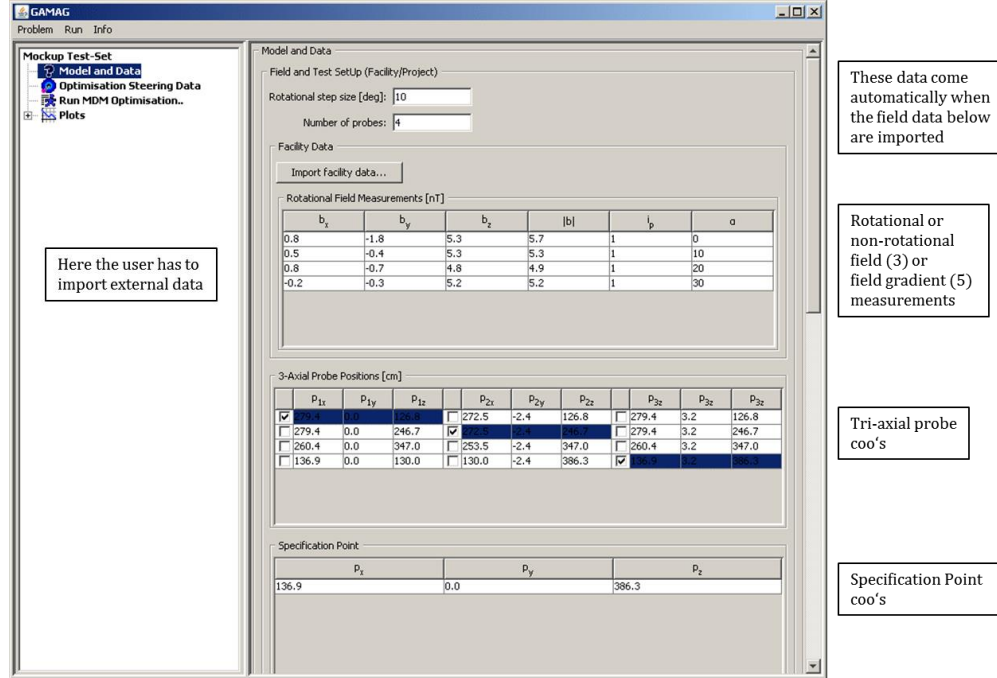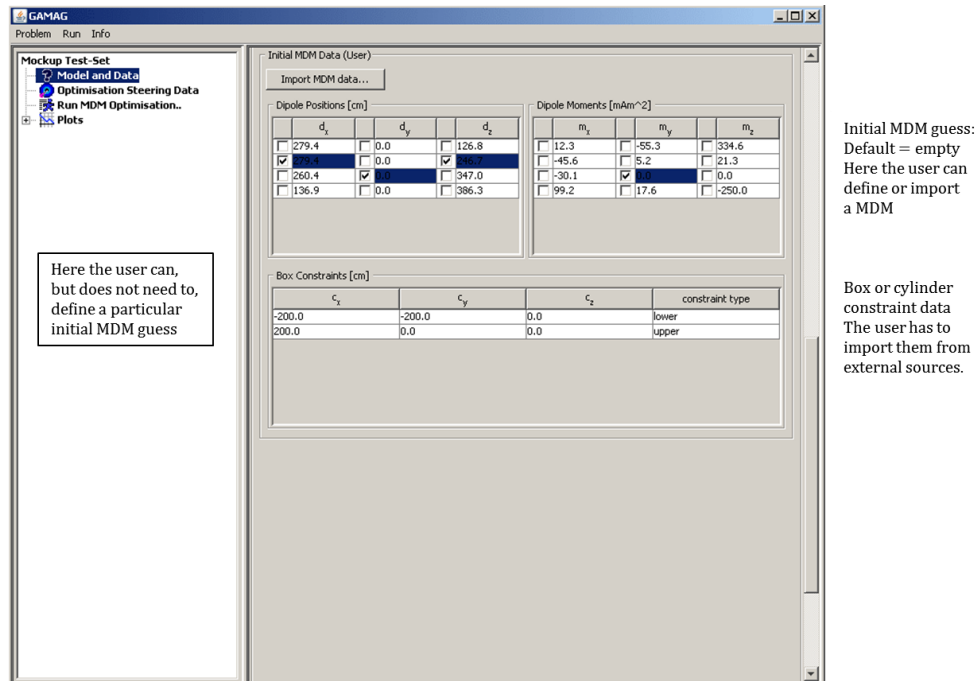

Fig.15 **GAMAG** GUI first page

Fig.16 **GAMAG** GUI second page

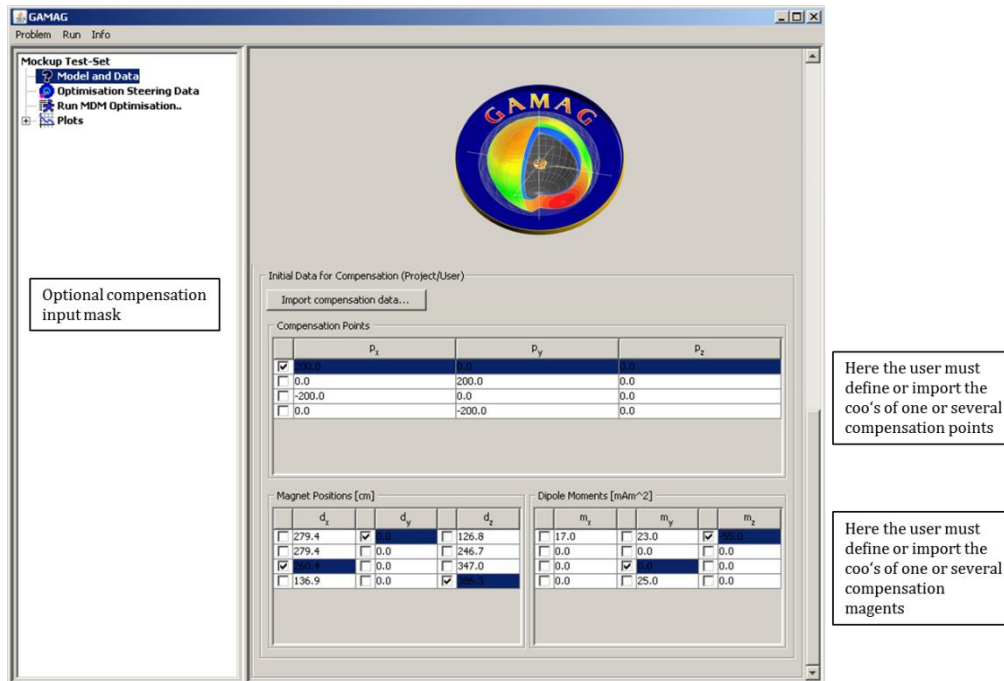Here the user can input an initial MDM guess but the default is none. The box constraints are again external data.

Fig.17 **GAMAG** GUI third page

On this page the user can import/insert data for the compensation magnet system in form of a MDM.
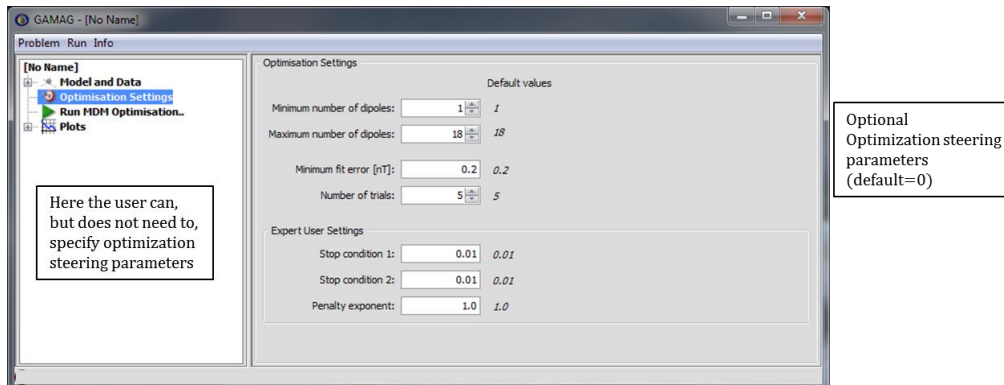
Fig.18 **GAMAG** GUI last page

This is the page where the normal user can change if he whishes a small set of optimzation steering parameters, and an expert user has here access to more special steering parameters.

It is important to note that in the nominal case the user has only to import external data in order to run a case. This means that the **GAMAG** software, except for pathological cases, runs automatically. This is the largest improvement w.r.t. the precursor version of the software.

5.2. GAMAG-B/Bg Graphical User Interface (GUI) Output

The output of a **GAMAG** run contains a detailed and self-explaining report and 2D and interactive 3D graphics.
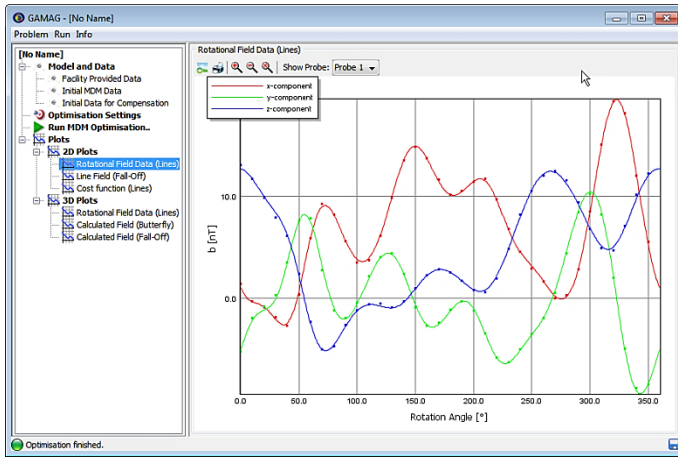
Fig.19 Carthesian plot
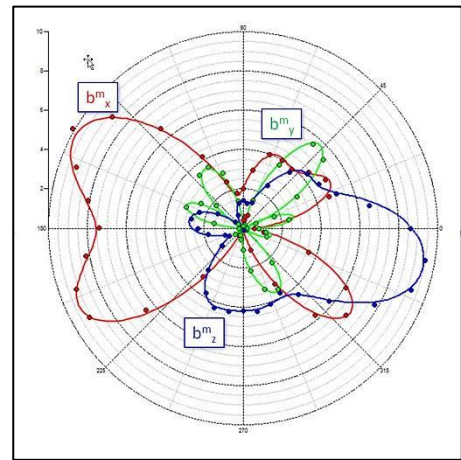
Fig.20 Polar plot
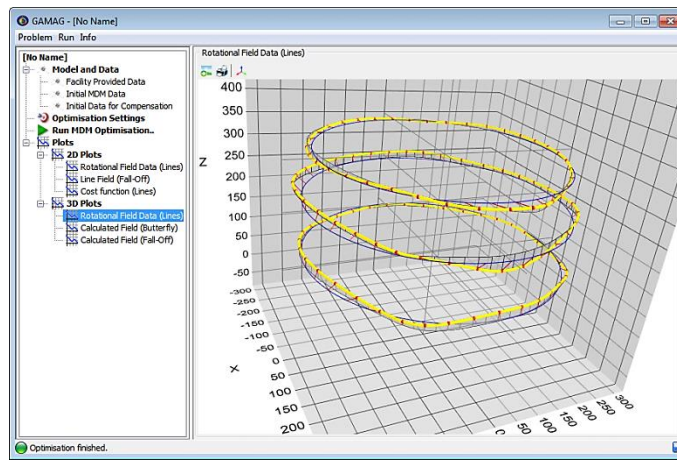
Fig.21 3D interactive data fit plot
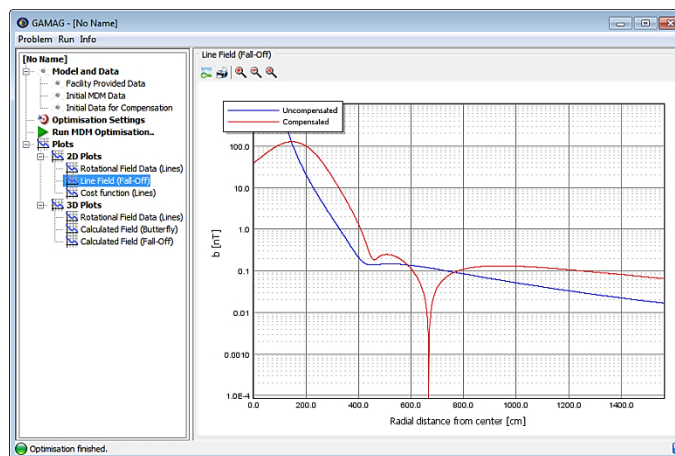
Fig.22 Carthesian Fall-Off plot
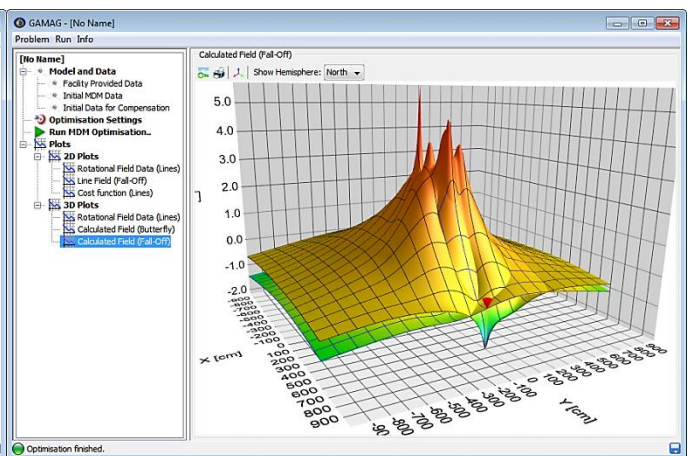
Fig.23 3D interactive Fall-Off plot

6.   GAMAG Add-On Software
6.1. GAMAG-SSCM Software

A spacecraft MDM built up by unit MDMs is called Synthetic Spacecraft Model. It is used for cleanliness control and, in the case a LCF is not available, it replaces a system test, of course with the risk of degraded accuracy.

Unit MDMs are described in the first instance in the Test Frame. Hence, in order to integrate them in the Synthetic Spacecraft Model they have to undergo a two-fold coordinate transformation:

1. Transformation from Test to Unit Frame
2. Transformation from Unit to Spacecraft Frame

As indicated on Fig.24 there are two translation vectors and two rotation matrices involved which have to be extracted from blueprints of the spacecraft. Note that the determination of the rotation matrices is particularly error-prone. These data together with the associated unit MDMs represent the input of the SSCM software which produces then the Synthetic Spacecraft MDM. In complex cases the spacecraft MDM can contain up to 200 dipoles.

The output of SSCM are

1. the Synthetic Spacecraft MDM
2. the associated global dipole moment of the spacecraft
3. the associated field at the magnetometer location of the spacecraft.
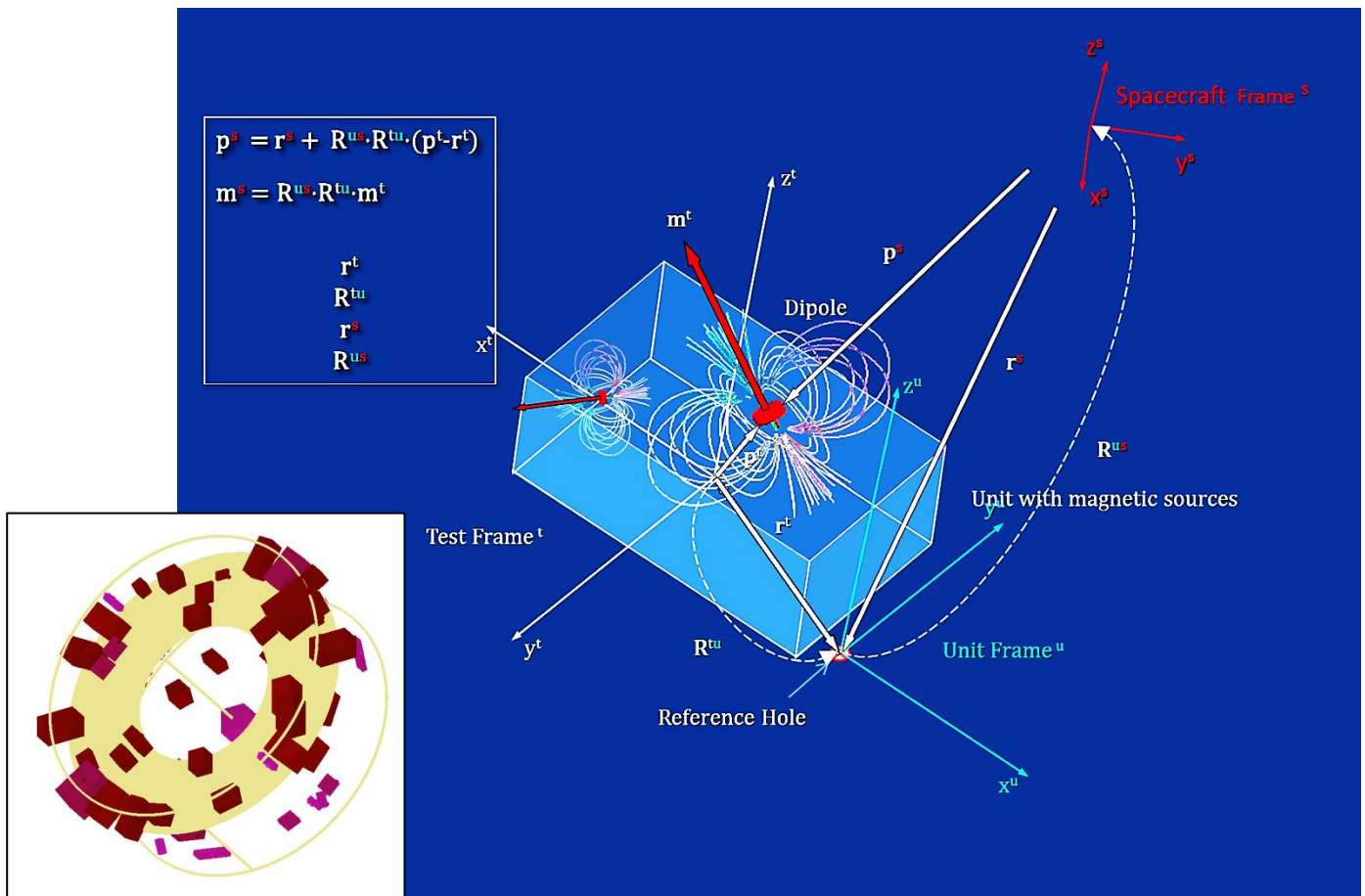
Fig.24 Coordinate transformation test to spacecraft frame

6.2. GAMAG-DIMAL Software

The GAMAG-DIMAL s/w allows a sophisticated and realistic control and prediction of the magnetic cleanliness of spacecraft, covering all phases of a project till the final system test. The name of the software stands for Dipole Moment Allocation List.

At the start of a project some units are quite well known from previous projects, some major contributors have to be identified by magnetic sniffing, and the rest has to be estimated by the moment allocation method.

In the following phases of the project more and more units become available for magnetic testing and for the determination of their MDM. In the budgeting process for unknown units only the global dipole moment vectors are considered. Their moment allocations are optimized in order to fit the field budget.

A magnetic review board would analyze the list frequently. In such a way early warnings arise when some units exceed the budget. Thereupon corrective actions can be defined, whether by changing critical ferromagnetic parts or electrical design (loops). When the involved units cannot be corrected for instance a magnetic compensation by magnets can be applied, as has been done for the Ulysses Travelling Wave Tubes and the Radioisotope Thermal Power Generator (RTG). In exceptional cases shielding with μ-metal can be applied. The allocation list is thus a budget household tool and it evolves throughout the projects development.

The allocation method distinguishes between three categories of units (Fig.25):
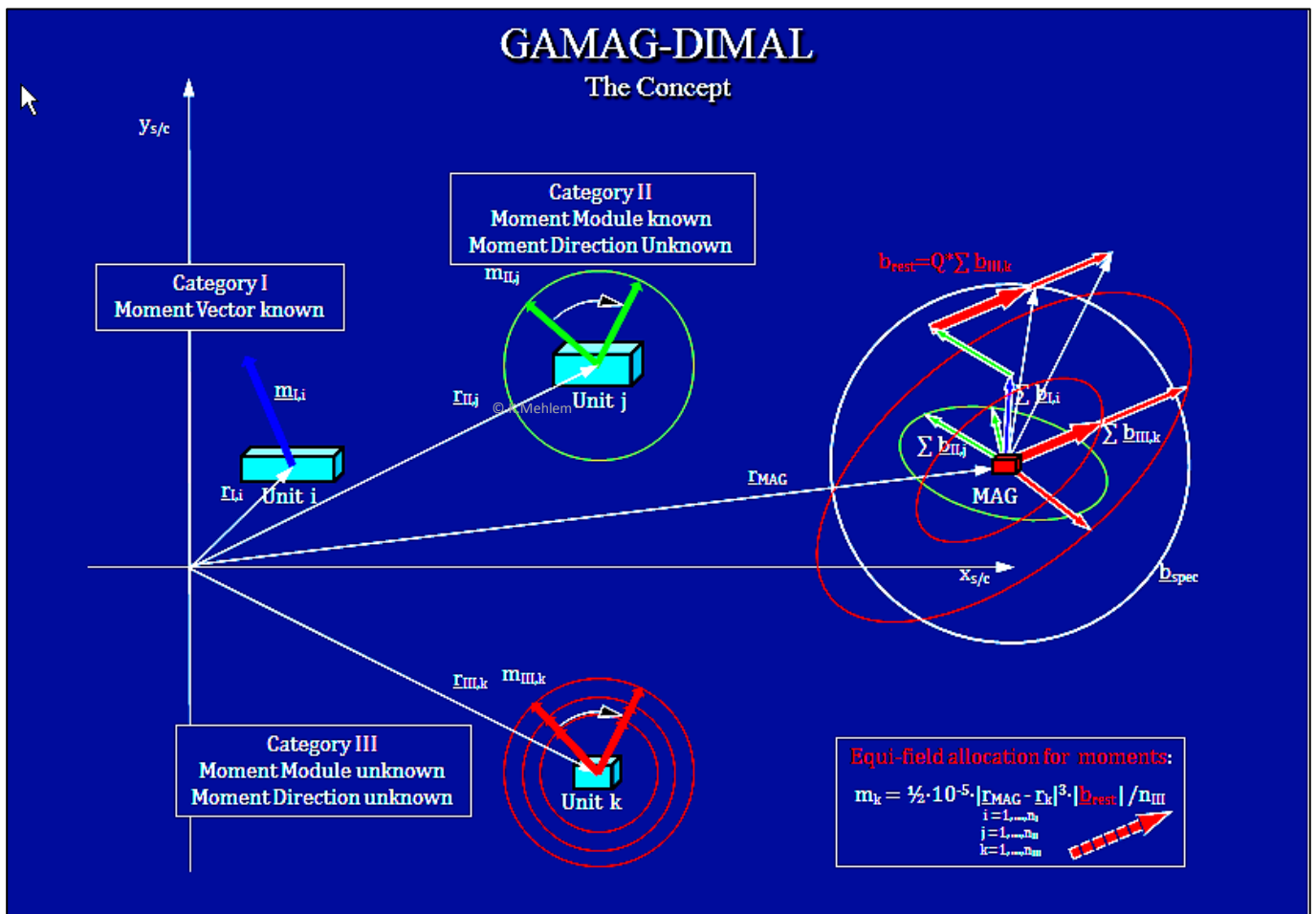
Fig.25 Concept of magnetic moment allocation

```
Input:
Total allocated field at MAG-location [nT]     =   25.
MAG-location [cm] in S/C frame                 = -225.0  75.0  33.9
Number of trials                               =  20000
Number of classes                              =    200
Confidence level [%]                           =  99.50


Legend of Output:
x,y,z    = unit coordinates in S/C frame [cm]
r        = distance between unit and MAG-location [cm]
b        = field of unit at MAG [nT] (FGP)
m        = unit moment [Gcm³ = 10⁻³Am² = mAm²] = max.allocation
CAT I    = known moment and unknown direction
Cat II   = unknown direction of known moment
Cat III  = unknown moment and unknown direction
FGP      = First Gaussian Position
```

Unit	x	y	z	r	b	m	
PDU P/L	29.1	-86.0	198.7	343.	0.0	10.	Cat II
PDU S/S	-68.7	-86.0	71.6	228.	0.2	10.	Cat II
BCU	56.0	-91.0	41.0	326.	2.1	366.	Cat III
Battery 1	86.5	-91.2	49.5	353.	0.0	10.	Cat II
Battery 2	86.5	-91.2	83.0	356.	0.0	10.	Cat II
Battery 3	61.0	-91.2	83.0	334.	0.1	10.	Cat II
SADM +y	0.0	91.1	132.0	246.	0.3	20.	Cat II
SADM -y	0.0	-91.1	132.0	296.	0.2	20.	Cat II
SADE	-21.5	-89.2	30.5	262.	0.1	10.	Cat II
Solar Array -y_1	0.0	-359.7	132.0	499.	0.2	125.	Cat I
Solar Array -y_2	0.0	-644.5	132.0	760.	0.1	125.	Cat I
Solar Array -y_3	0.0	-929.3	132.0	1034.	0.0	125.	Cat I
Solar Array -y_4	0.0	-1214.1	132.0	1312.	0.0	125.	Cat I
Solar Array -y_5	0.0	-1498.9	132.0	1593.	0.0	125.	Cat I
Solar Array +y_1	0.0	359.7	132.0	376.	0.5	125.	Cat I
Solar Array +y_2	0.0	644.5	132.0	620.	0.1	125.	Cat I
Solar Array +y_3	0.0	929.3	132.0	889.	0.0	125.	Cat I
Solar Array +y_4	0.0	1214.1	132.0	1165.	0.0	125.	Cat I
Solar Array +y_5	0.0	1498.9	132.0	1445.	0.0	125.	Cat I
TWT1	60.0	93.5	58.5	287.	2.1	248.	Cat III
TWT2	60.0	93.5	43.5	286.	2.1	246.	Cat III
EPC1	20.5	91.5	66.9	248.	2.1	161.	Cat III
EPC2	20.5	91.5	20.5	246.	2.1	158.	Cat III
Transponder A	20.8	89.2	90.1	253.	0.1	10.	Cat II
Transponder B	20.8	89.2	43.7	246.	0.1	10.	Cat II
RFDU	90.7	94.0	60.0	317.	0.1	10.	Cat II
WIU	75.5	92.0	25.5	301.	2.1	287.	Cat III
USO	85.5	89.5	130.0	325.	0.1	10.	Cat II
HGA	213.5	0.0	8.0	446.	0.0	0.	--/--
MGA-X	117.3	-55.0	243.0	422.	0.0	0.	--/--
MGA-S	117.3	55.0	243.0	402.	0.0	0.	--/--
LGA1	90.0	0.0	310.5	426.	0.0	0.	--/--
LGA2	-111.0	-50.0	-0.6	173.	0.0	0.	--/--
APME	22.5	-89.5	32.5	297.	0.1	10.	Cat II
SSMM	81.5	87.5	164.0	333.	0.1	20.	Cat II
RTU P/L	-55.5	89.5	210.0	245.	0.3	20.	Cat II
RTU S/S	-25.0	89.5	77.5	205.	0.5	20.	Cat II
CDMU1	-76.9	87.1	42.8	149.	2.1	35.	Cat III
CDMU2	-76.9	87.1	77.2	155.	2.1	39.	Cat III
AIU	-25.0	89.5	42.5	201.	2.1	85.	Cat III
WDE	59.3	90.5	83.0	289.	0.1	10.	Cat II
RW1	75.0	20.0	130.0	320.	2.1	344.	Cat III
RW2	75.0	20.0	90.0	310.	2.1	314.	Cat III
RW3	75.0	-20.0	130.0	329.	2.1	375.	Cat III
RW4	75.0	-20.0	90.0	320.	2.1	344.	Cat III
Gyro Unit 1	-20.0	-90.5	58.8	265.	2.1	195.	Cat III
Gyro Unit 2	-20.0	-90.5	83.8	268.	2.1	203.	Cat III
Gyro Unit 3 - tbd	0.0	0.0	0.0	240.	2.1	145.	Cat III
Nav + SST Elec1.	-44.5	93.0	150.0	215.	0.2	10.	Cat II
Nav + SST Elec2.	-44.5	-93.0	150.0	273.	0.1	10.	Cat II
Nav. 1	-90.0	0.0	210.0	234.	0.2	10.	Cat II
Nav. 2	-90.0	25.0	210.0	227.	0.2	10.	Cat II
Sun Sensor 1	55.0	55.0	294.0	383.	0.1	20.	Cat II
Sun Sensor 2	108.5	0.0	250.0	404.	0.1	20.	Cat II
Sun Sensor 3	-119.0	40.0	0.0	117.	2.5	20.	Cat II
Sun Sensor 4 - tbd	0.0	0.0	0.0	240.	0.3	20.	Cat II
Star Tracker R	-90.0	-57.5	190.0	245.	0.3	20.	Cat II
Star Tracker L	-90.0	57.5	190.0	207.	0.5	20.	Cat II
Thruster 1 Nom.	-121.8	-106.0	216.7	277.	2.1	224.	Cat III
Thruster 1 Red.	-121.8	-106.0	205.7	270.	2.1	207.	Cat III
Thruster 2 Nom.	121.8	-106.0	216.7	432.	2.1	847.	Cat III
Thruster 2 Red.	121.8	-106.0	205.7	427.	2.1	821.	Cat III
Thruster 3 Nom.	-121.8	-106.0	216.7	277.	2.1	224.	Cat III
Thruster 3 Red.	-121.8	-106.0	205.7	270.	2.1	207.	Cat III
Thruster 4 Nom.	121.8	-106.0	216.7	432.	2.1	847.	Cat III
Thruster 4 Red.	121.8	-106.0	205.7	427.	2.1	821.	Cat III
Thruster 5 Nom.	121.8	106.0	216.7	393.	2.1	640.	Cat III
Thruster 5 Red.	121.8	106.0	205.7	388.	2.1	616.	Cat III
Thruster 6 Nom.	-121.8	106.0	216.7	212.	0.0	0.	--/--
Thruster 6 Red.	-121.8	106.0	205.7	203.	0.0	0.	--/--
RPC IAP UPPER	-230.8	195.6	419.3	404.	2.1	693.	Cat III
RPC IAP LOWER	-233.8	188.8	13.0	116.	2.1	16.	Cat III
RPC MIP	-192.9	157.9	365.7	344.	2.1	427.	Cat III
VIRTIS Elec.	-44.3	-88.0	240.5	319.	0.1	10.	Cat II
VIRTIS PMH.	-83.8	-94.5	248.3	308.	2.1	306.	Cat III
VIRTIS PEMM.	-84.7	-92.2	220.5	287.	2.1	249.	Cat III
VIRTIS Sensor	-124.6	-65.9	235.0	265.	2.1	197.	Cat III
SREM	87.1	-90.9	22.6	354.	2.1	466.	Cat III
SSP Proc.	-58.0	92.0	170.0	216.	2.1	106.	Cat III
SSP TX	-98.0	55.0	240.5	243.	0.1	10.	Cat II
SSP RX	-98.0	75.0	240.5	243.	0.1	10.	Cat II
SSP ANT1	-78.0	56.0	266.0	275.	0.0	0.	--/--
SSP ANT2	-58.0	25.0	266.0	290.	0.0	0.	--/--
SSP Lander	-124.8	0.0	152.8	173.	0.0	0.	--/--

```
Fields at MAG location:
Field from Cat I moments                       =    0.6 nT
Field from Cat I+Cat II moments      (FGP)     =    7.2 nT
Field from Cat I+Cat II moments      (50%)     =    1.8 nT
Field from Cat III moments           (FGP)     =  106.4 nT
Field from Cat II+Cat III moments    (FGP)     =  113.3 nT
Worst case field from all moments    (FGP)     =  113.9 nT
Total field allocation (Spec)                  =   25.0 nT
Total field at 99.50% confidence level         =   25.1 nT
```

The Category I comprises all units or parts which are quite well known from previous projects, like travelling wave tubes or thrusters etc. Their moment vectors are considered as fix.

The Category II comprises all units whose modules of the moments are known from experience, but whose directions are unknown. The directions are then subject of the moment allocation by stochastic evaluation.

Finally the Category III comprises all those units whose moment vectors are completely unknown and which are thus the subject of the moment allocation by stochastic evaluation of both module and direction.

The statistical evaluation uses Monte Carlo simulations where the unknown directions of the moment vectors are assumed to be distributed uniformly on a sphere.

The calculations are done in four steps:

1. Assume that all Cat.III moment vectors are pointing in first Gaussian direction (worst case).

2. Establish a large population of trials and derive the mean and the 3σ values of the field at the spacecraft magnetometer location.

3. Determine by iterative steps the optimal reduction-factor λ to be applied to the Cat.III moments such that total field norm generated by the vector sum of the moment vectors of all categories does not exceed the given field budget at a probability level of 3σ.

4. Divide the Cat.III total field in n equal parts and calculate the associated Cat.III moment norms via the inverse cubic law, taking thus the distance into account (see Fig.31 frame lower right corner).

Hence the so allocated moment norms guarantee implicitly that the field cleanliness specification is nor exceeded at a probability level of 3σ.

An example of an allocation list is shown on the adjacent figure.
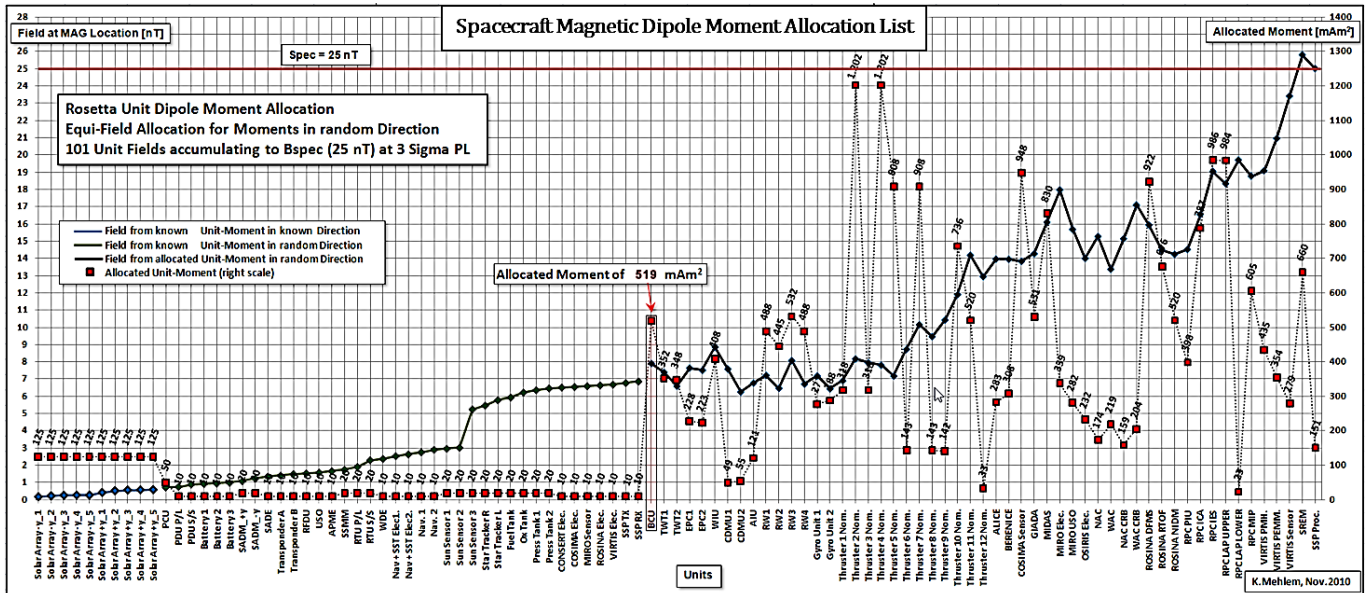
Fig.26 Allocation list

Fig.27 Example out of the compatible population of field contributions

6.3. **GAMAG-TSUCONF Software**

The precision of an MDM depends partly on the data coverage of the test article. A practical problem is that in practice only a few magnetometers, say 4-6, are available. Unfortunately, many tests have been conducted in the past without investigating seriously the question how to place the magnetometers so as to reduce the MDM Ambiguity Error.

GAMAG-TSUCONF is a tool to calculate the uniform distribution of n facility probes on a sphere.

When using a reference MDM it is then possible to determine, by reverse engineering, the minimum necessary number of points, and hence the angular separation $\Delta\beta$ (distance between red points), which leads to an allowable maximum MDM Ambiguity Error (see Fig.28, light blue surface regions).
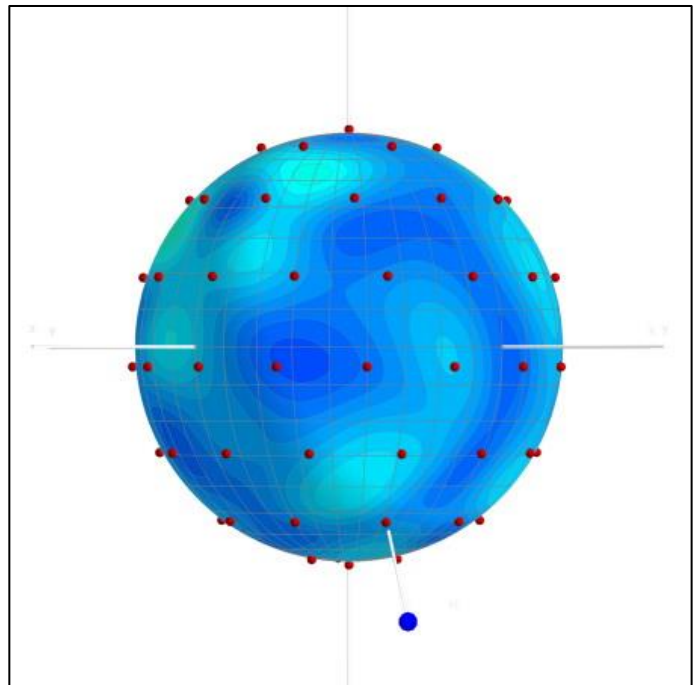
Fig.28 Reduced MDM Ambiguity Error by uniform distribution of measurement points

When the rotational measurement mode is chosen then the so found angular separation $\Delta\beta$ leads to the required number of probes $n_p=180/\Delta\beta+1$ (here $n_p=8$). The rotational step size $\Delta\alpha$ should then be smaller or equal to the separation $\Delta\beta$.

Fig.29 shows that for a given reference MDM it is recommended to use for the rotational mode at least 7 probes equally spaced from pole to pole in order to reduce MDM Ambiguity Errors substantially.
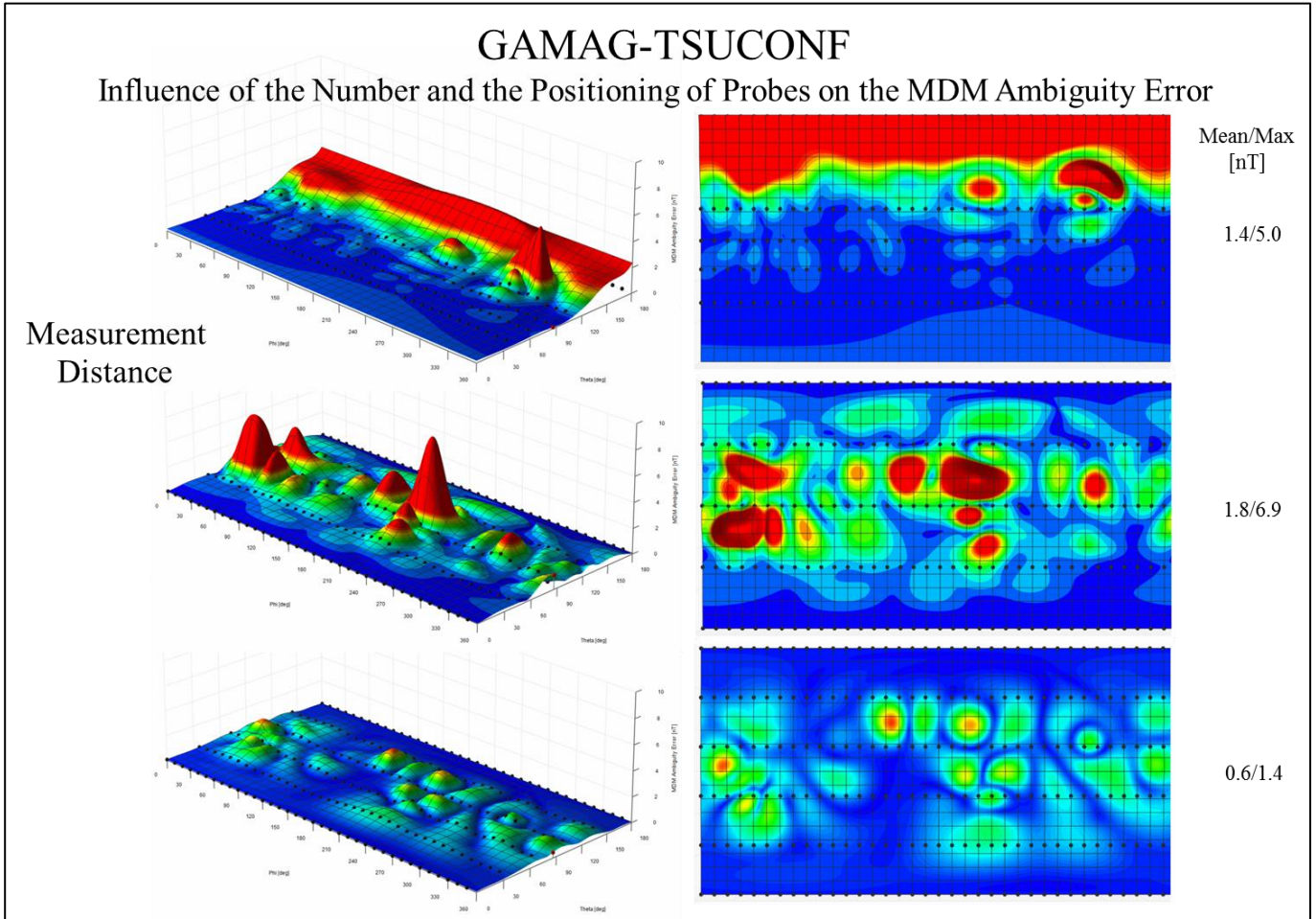
Fig.29 Optimal probe positioning w.r.t. MDM Ambiguity Error Reduction

6.4. GAMAG-TSUCAL Software

Once the probes have been installed a serious problem arises. For a MDM precision of 1% (dipole moment = 100 mAm^2 measurement distance = 50 cm) the required numerical probe positioning accuracy is 1,7 mm. This is difficult to be achieved manually. Also reading errors occur occasionally.

The GAMAG-TSUCAL software offers the possibility to identify the coordinates of the magnetic centers of the probe elements. For this

1. the probes have to be installed but it is not required to put them at precise locations,
2. a prior calibrated magnet or an active coil (Fig.30) is centered on the turntable,
3. rotational measurements are performed and read by the TSUCAL software,
4. starting from an approximate guess of the probe coordinates the software determines the exact magnetic centers of the probe elements by use of the GAMAG NLP solver.
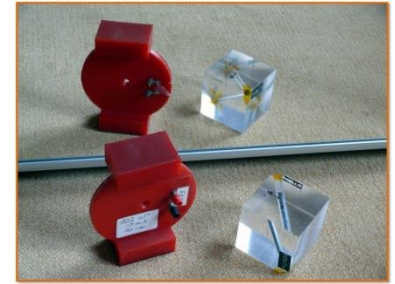
Fig.30 Calibration tools

The advantage of this approach is twofold:

1. the magnetic centers are determined with higher accuracy than by hand measurements,
2. if these field measurements, together with the coordinates and the used moment vector of the calibration device, are archived together with the actual field measurements of the test article, then it is in case of doubt later always possible by use of the TSUCAL software to re-identify the exact associated coordinates of the probe elements used. TSUCAL is not a stand-alone software but rather incorporated in the GAMAG-B software and it can be activated through the GUI.

Before: Initial Guess of Probe Positions [cm]: (rms of residues = 5.59 [nT])

		Element 1			Element 2			Element 3	
	P_x	P_y	P_z	P_x	P_y	P_z	P_x	P_y	P_z
1	50.0	0.0	50.0	50.0	0.0	50.0	50.0	0.0	50.0
2	50.0	0.0	50.0	50.0	0.0	50.0	50.0	0.0	50.0
3	50.0	0.0	50.0	50.0	0.0	50.0	50.0	0.0	50.0
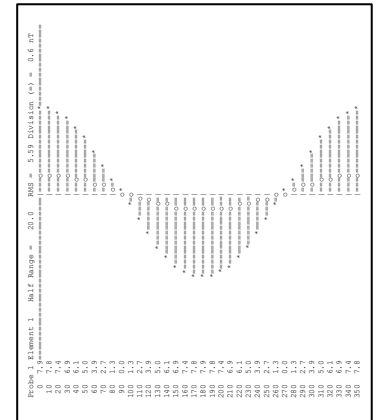
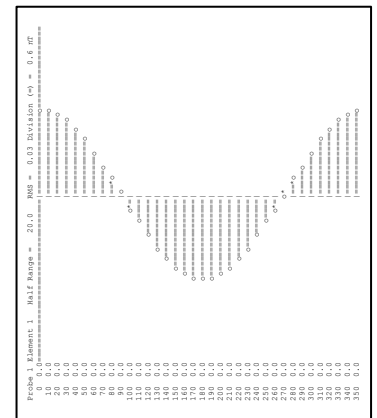Fig.31/32 Data fit before and after

After: Optimal Probe Positions [cm]:   (rms of residues = 0.03 [nT])

		Element 1			Element 2			Element 3	
	P_x	P_y	P_z	P_x	P_y	P_z	P_x	P_y	P_z
1	60.6	0.0	30.3	60.6	0.0	30.3	60.6	0.0	30.3
2	60.6	0.0	0.0	60.6	0.0	0.0	60.6	0.0	0.0
3	60.6	0.0	-30.3	60.6	0.0	-30.3	60.6	0.0	-30.3

7. Examples of GAMAG Applications

7.1. Giotto

The famous European spacecraft Giotto, which was the first spacecraft to approach a comet, passed close to the comet Halley in 1986. It carried two magnetometers mounted on one leg of a so-called antenna tri-pot (Fig.38). A pair of strongly magnetic Travelling Wave Tubes (TWT's) located on the upper platform and at a distance of only 1,47m from MAG-1, generated a perturbing field of 39.3 nT which would have severely polluted the magnetometer readings during. It had been decided that this pair had to be compensated by use of a magnet.

In a first step three candidate TWT combinations (composed of 2 flight models and 1 spare) were mapped in the CNES magnetic test facility and precise MDM's were derived. In a second step the fields at MAG-1 for all three possible TWT combinations were calculated. In a third step the associated optimal compensation magnet moment vectors were determined.

One combination was finally selected as flight hardware. A 6 cm long magnet of 1139 mAm^2 was fabricated and then installed on a bracket next to the TWT pair. This composite was then mapped and modeled again, confirming precisely the predicted compensation effect. Since the distance between the composite and MAG-1 was only 1.47m, we had the rare opportunity to check the compensation effect directly by a measurement at the equivalent MAG-1 location. The field readings in all three axes were quasi zero, such that the facility engineer thought that he had forgotten to switch on the facility magnetometer. This test was an excellent validation of the MDM approach.
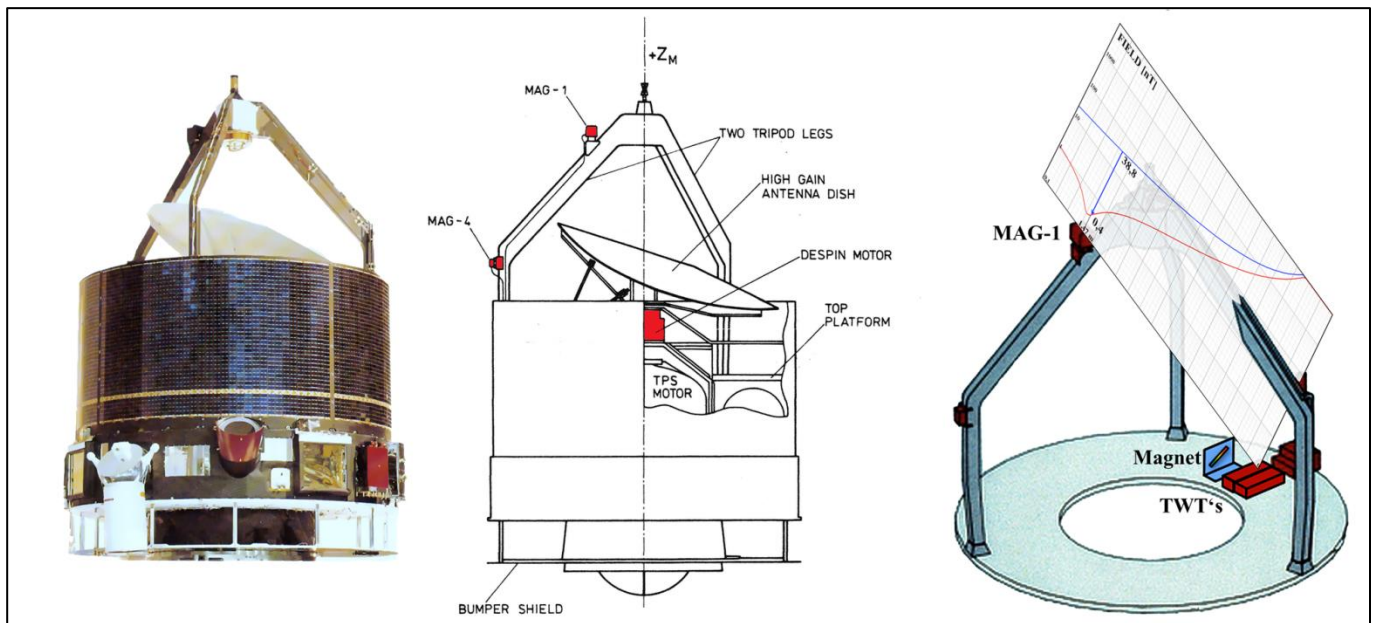

Fig.33 Giotto dual-TWT field compensation at MAG-I by use of a strong magnet (blue and red curve)

7.2. <u>Ulysses</u>

After 19 years of spectacular discoveries the Ulysses spacecraft travels still around the sun on a polar orbit. It carries a Fluxgate Magnetometer (FGM) and a Vector Helium Magnetometer (VHM) at a distance of 6.45m from the spacecraft center. The cleanliness specification of 0.1 nT at the VHM location, was the strongest one ever imposed.

The modeling task was made more difficult than usual because the spacecraft could not be rotated with its boom extended (Fig.41 insert) and because the Radioisotope Thermoelectric Power Generator (RTG) of NASA could for evident reasons not be present during the magnetic test at IABG, Germany.

The RTG was tested separately at EG&G in Miamisburg, Ohio, USA, prior to the system test at IABG (Fig.34). Since the RTG was for safety reasons not allowed to be moved to a coil facility, the tests had to be performed in the unshielded magnetic environment of the EG&G plant. Even after careful calibration of the probes the field measurements were plagued by field off-sets which did not allow a satisfactory modeling. Thanks to the gimbaled RTG fixture on the turn table, it was possible to map the RTG in two orthogonal planes. The tangential elements of the measured field vectors were then used to derive an accurate MDM and the associated field vector at the Ulysses VHM location was calculated. Thereupon a compensation magnet was determined, manufactured on-site and fixed with a bracket on one fin of the RTG. Further mapping and modeling with the magnet installed confirmed the compensation effect accurately.
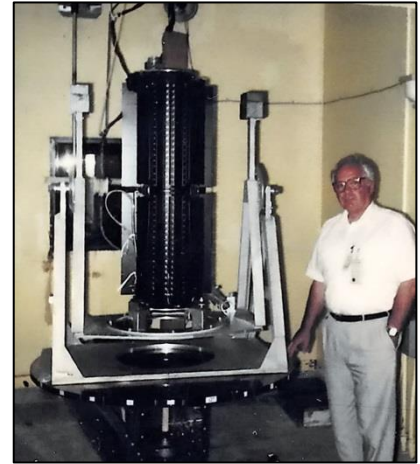
Fig.34 RTG, author, mag.test

A pair of highly magnetic TWT's, located under the antenna dish of Ulysses, had been compensated prior to integration. Since the spacecraft with extended boom was too large for rotational measurements, it had to be tested in two separate modes. First, the spacecraft was tested in the rotational mode with the boom in the stowed configuration. Some significant field warping appeared, which was quite a challenge for the modeling. It was caused by two magnetic experiments (URAP and GRB) which were fixed on the boom close to the boom hinge (Fig.35). Since the spacecraft was magnetically quite clean (no RTG, TWT's compensated), an acceptable SNR could only be obtained close to the spacecraft body. This meant that the URAP experiment unit passed very closely (40cm) by the facility probes during rotation.

The URAP MDM had to be identified separately by use of a so-called linear fall-off scan of the extended boom. It was then transformed into the stowed boom configuration and subtracted from the spacecraft MDM (boom stowed). Then it was added to the spacecraft MDM in extended boom configuration. Finally, the MDM of the RTG was also added.

The total S/C MDM contained 35 dipoles. The figures 36 and 37 show the spacecraft field with the RTG and the TWT's uncompensated and compensated (918 pT and 76 pT at the FGM location and 566 pT and 45 pT at the VHM location). The 45 pT have in fact been confirmed in flight and the spacecraft was declared as the cleanest one ever flown.
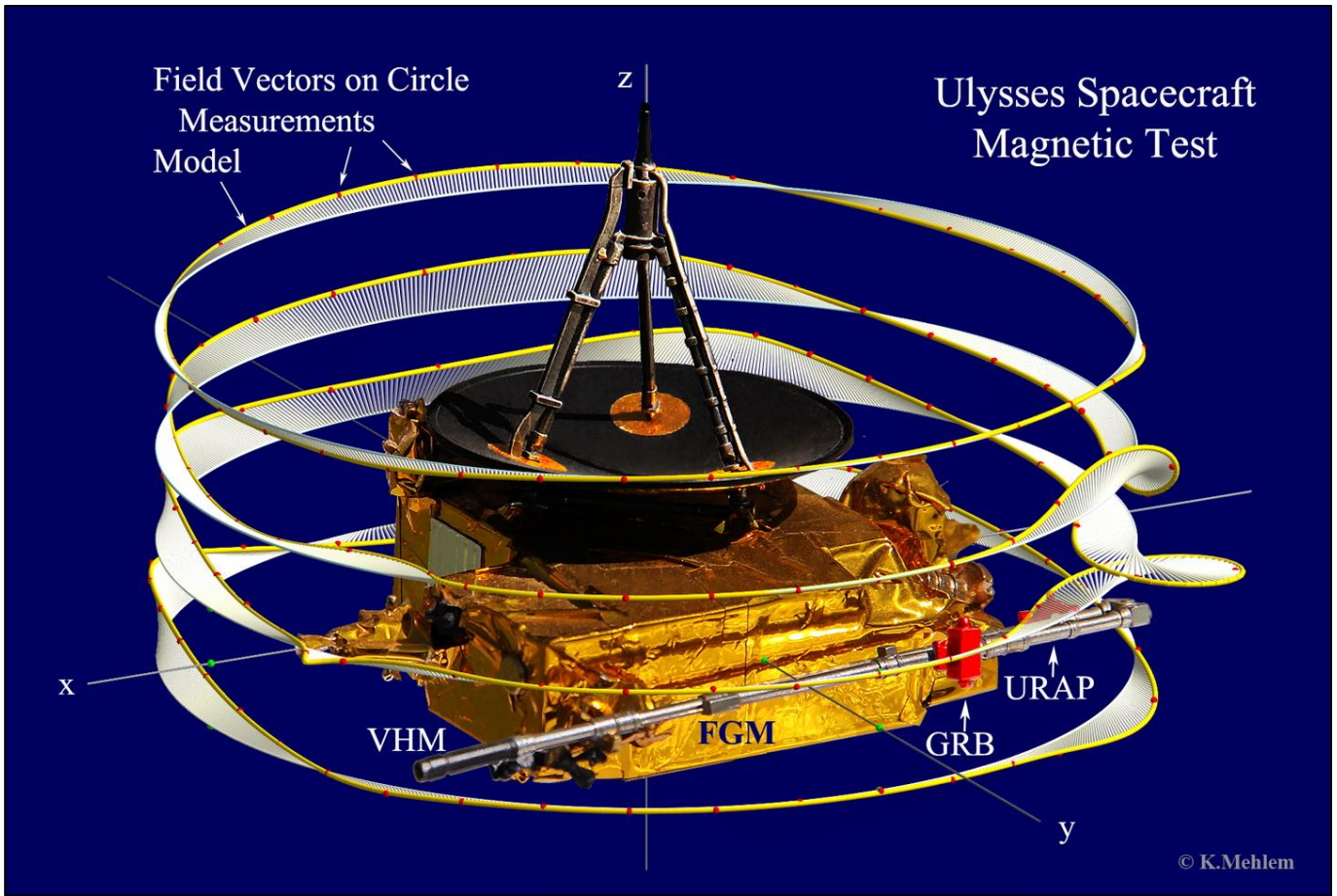
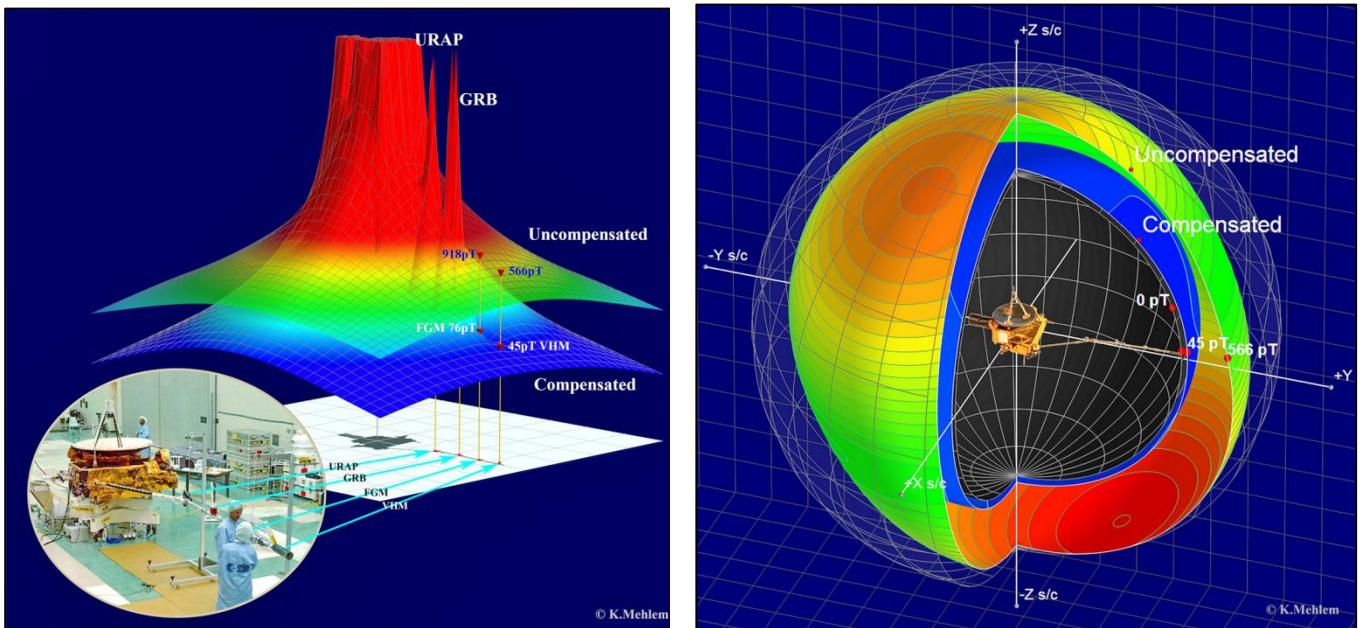Fig.35 Ulysses in test configuration (boom stowed)

Fig.36/37 Ulysses before and after field compensation (VHM)

7.3. Cluster

The four Cluster spacecraft explore the magnetic field around the Earth in a formation flight. The magnetic cleanliness specification for the location of the outboard Fluxgate Magnetometer (FGMO) was set to 0.25 nT. In order to achieve this value, the four spacecraft went through the most intensive magnetic cleanliness program ESA has ever carried out. Each of the four spacecraft had a number of magnetically critical units and sub-assemblies (like thruster-valves etc.). In a preparatory phase every unit was mapped and modeled by using a small ESA coil facility (Fig.7) and the precursor of the **GAMAG-B.** A synthetic spacecraft MDM was successively built up. Fig.3 depicts critical units on board the Cluster spacecraft. Each complete spacecraft was tested in the large Helmholtz coil facility of IABG, Germany, Fig.4) in at least four magnetic states. The optimal MDM's for all rotational measurements and the associated fields at the FGMO had to be calculated live during the test. Since most of the magnetic units were located on the rim of the spacecraft a minimum of 12 dipoles were required per MDM.
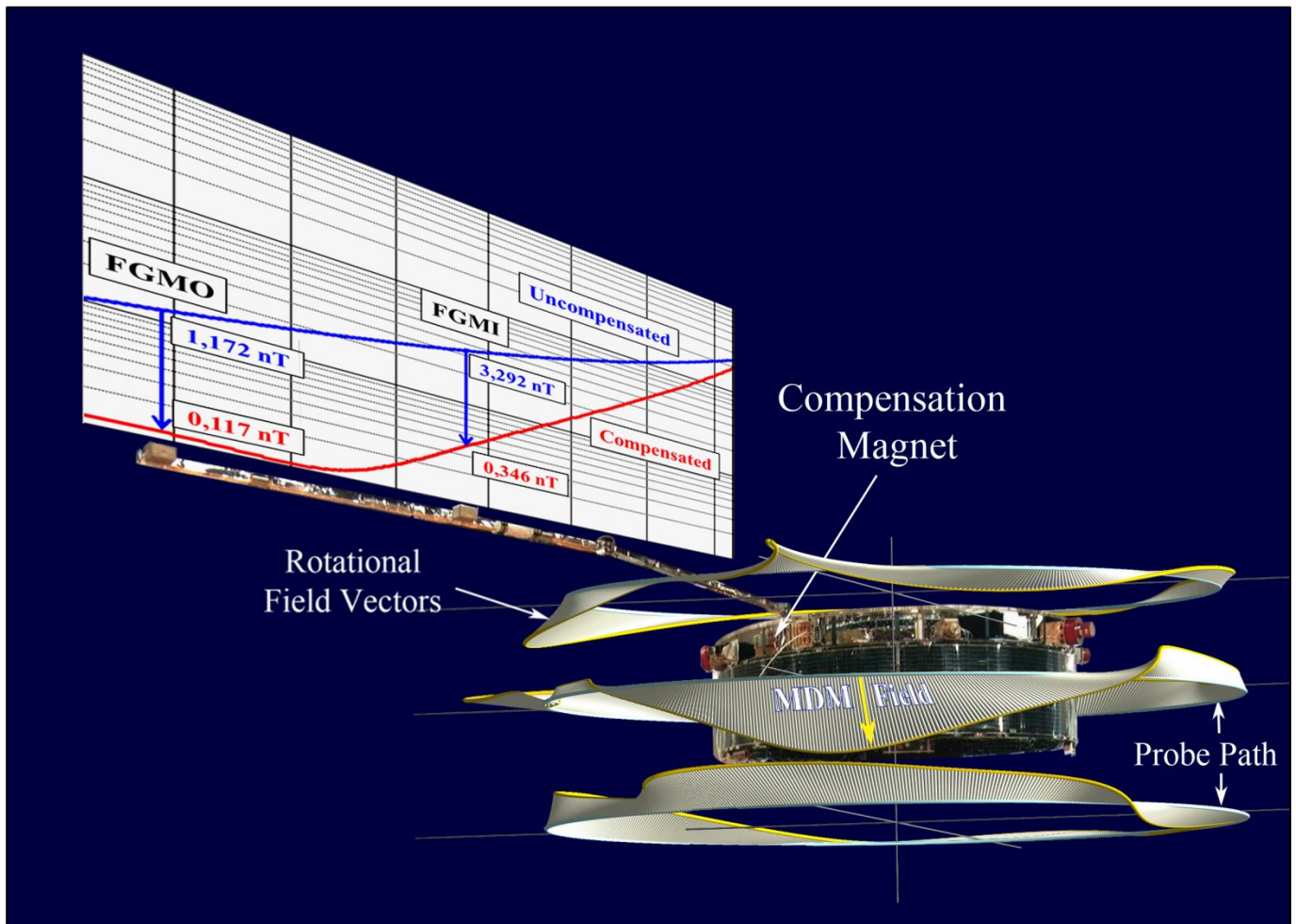

Fig.38 Cluster before and after field compensation (FGMI and FGMO)

As the magnetic cleanliness specification of 0.25 nT was exceeded, a magnet had to be determined for the compensation of both the FGMI and the FGMO field. The corresponding magnet had to be split into two parts because only two orthogonal surfaces were available for the installation of the magnets. A so-called x,y-magnet with the components $[m_x, m_y, 0]$ had to be fixed on a small horizontal surface of the spacecraft at a position $\mathbf{p}_1$. A so-called z-magnet with the components $[0, 0, m_z]$ had to be fixed on a small vertical bracket installed on the spacecraft at a position $\mathbf{p}_2$. The moment vectors of both magnets had been optimized. Since we had 3 moment components to generate in total 6 compensating far-field vectors, only a least square solution was possible. Nevertheless, a reduction of the field by an order of

magnitude at both locations was achieved (Fig.38). It had then to be verified by a new measurement-modeling cycle. Each of the four spacecraft needed compensation. After the tragic launch failure of Ariane V and the loss of all four Cluster spacecraft, the recovery project Cluster II was started. The same cleanliness program was successfully repeated. In total about 50 spacecraft MDM's were derived and all spacecraft were successfully compensated for FGMI and FGMO, each by use of one magnet only.

7.4. Cassini

Orbiting Saturn Cassini carries two magnetometers (one VHM, left, and one FGM, mid) on an 11 m long deployable boom. The target cleanliness level was set to 200 pT at the VHM location. The spacecraft is powered by three RTG's (F2, F6, F7) magnetically similar to the one carried by Ulysses.

A series of complex mapping exercises were performed in the industrial and radioactive environment of the EG&G facility in Miamisburg, Ohio, USA. All RTG's had been modeled by the author during the tests. When building the synthetic model of all three RTGs it turned out that in the worst case the RTG's would generate up to 115 pT at the VHM location, which is more than half of the whole spacecraft allocation (200 pT). In an effort to avoid the use of compensation magnets for each RTG, the author found out that if each RTG could be installed at any of the three locations and if clocking angles of 30 degrees were allowed, a substantial field self-compensation of > 90% at the VHM location was attainable.

RTG Position	1	2	3	
Clocking Angle	ϕ_1	ϕ_2	ϕ_3	$|b|_{VHM}$
	degrees			pT

RTG Configuration	F2	F6	F7	
nominal	150	0	0	72
minimum	-30	60	-90	17

RTG Configuration	F2	F7	F6	
nominal	150	0	0	73
minimum	-30	60	-90	16

RTG Configuration	F6	F2	F7	
nominal	150	0	0	49
minimum	-120	90	-60	4

RTG Configuration	F6	F7	F2	
nominal	150	0	0	116
minimum	-30	-150	60	25

RTG Configuration	F7	F2	F6	
nominal	150	0	0	45
minimum	-120	90	-30	8

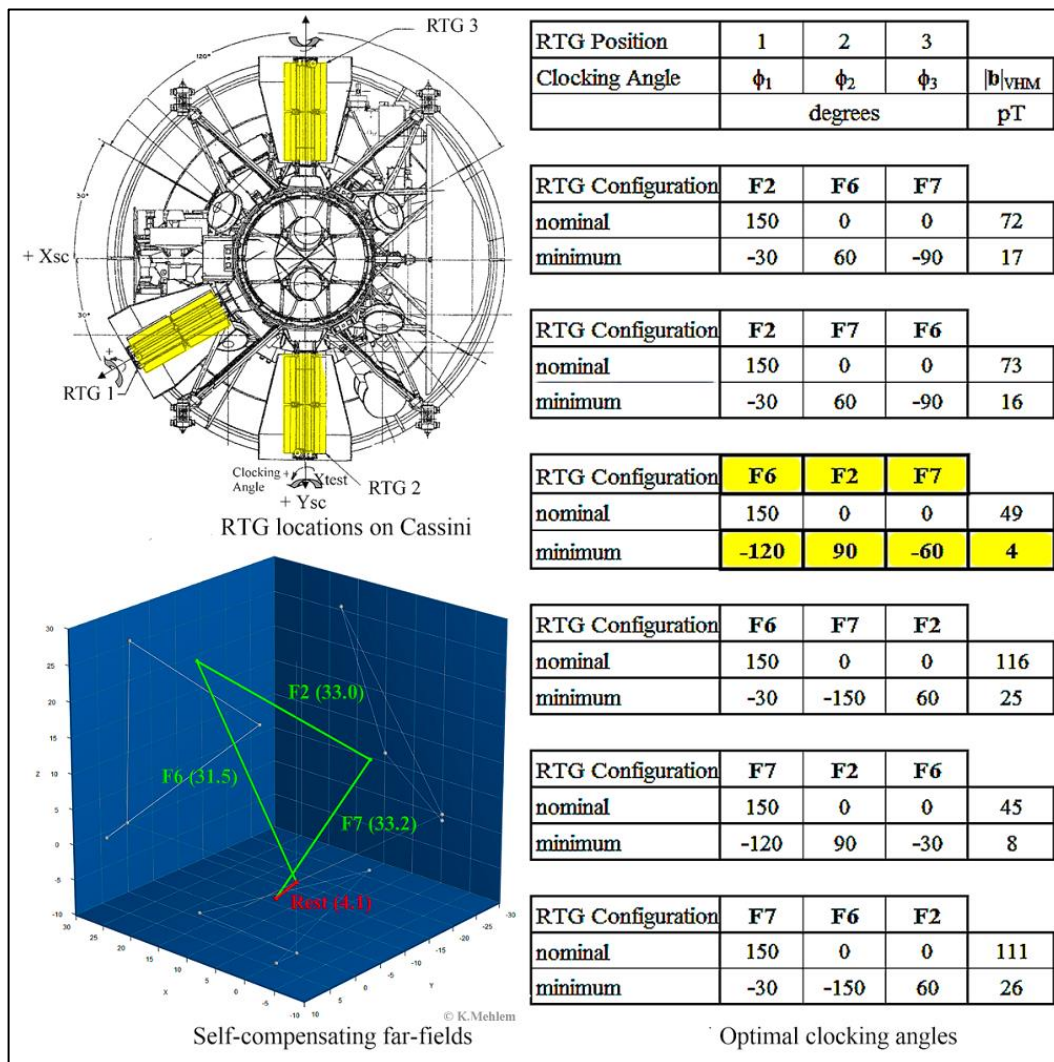| RTG Configuration	F7	F6	F2	
nominal	150	0	0	111
minimum	-30	-150	60	26

Fig.39 Cassini optimal positions and clocking angles for the RTG installation
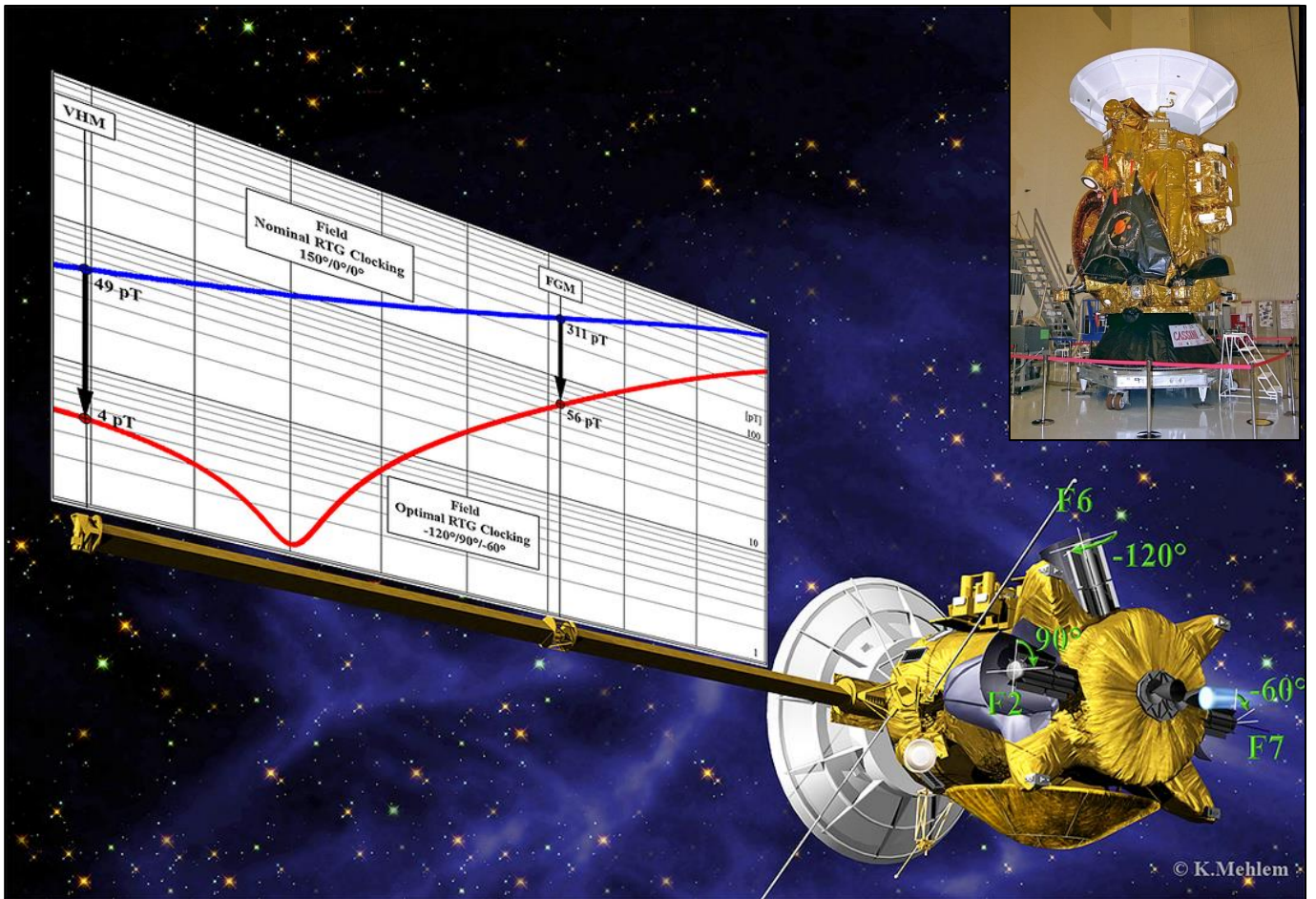
Fig.40 Cassini before and after field compensation at the outboard magnetometer (FGMO)

The prescriptions were finally implemented and in-flight measurements later confirmed the success of this compensation exercise. It represents a classical example of efficient self-compensation techniques.